Heliyon 9 (2023) e18361

Contents lists available at ScienceDirect

Heliyon

journal homepage: www.cell.com/heliyon

Detailed urban roughness parametrization for anthropogenic heat flux estimation using earth observation data

Manushi M. Bhatt [a], Kshama Gupta [a,*], Abhishek Danodia [a], Surya Deb Chakroborty [b], N.R. Patel [a]

[a] Indian Institute of Remote Sensing, 4 Kalidas Raod, Dehradun, Uttrakhand, India
[b] Environmental Systems Research Institute, Kolkata, West Bengal, India

ARTICLE INFO

Keywords:
Anthropogenic heat
Urban energy balance
Urban roughness
Large aperture scintillometer
Delhi region

ABSTRACT

Anthropogenic Heat (AH) emissions modify the energy balance in urban areas and is crucial for urban microclimate modelling and improved weather forecast modelling. Therefore, the present study conducted on Delhi and its surroundings firstly aims to estimate AH using Earth Observation (EO) data of Landsat 8 then, evaluate the impact of detailed urban roughness parameterization on the estimation of AH and further validate the obtained flux values with ground based observations of Large Aperture Scintillometer (LAS) setup. The study has been conducted over three time periods for October 2017, March 2018 and June 2018 by processing six Landsat tiles. Three methods have been employed on EO data for AH computation i.e. single urban roughness value for entire study area (Method 1), LULC based roughness values adopted from the literature (Method 2) and lastly, detailed pixel-by-pixel varying roughness values calculated from fine scale urban parameterization (Method 3) for each time period, The average AH values are higher for the month of June 2018: 359.91, 368.57 and 359.16 W/m^2 as compared to month of March 2018 (322.44, 330.84 and 298.35 W/m^2) and October 2017 (318.00, 331.04 and 306.71 W/m^2) for method 1, method 2 and method 3 respectively. Net radiation and Sensible Heat Flux shows a good correspondence with in-situ measurements for most of the tiles and method 3 shows better spatial distribution of fluxes as compared to other two methods. However, due to difference in approach for estimation of fluxes (LAS setup computes latent heat flux as residual while EO based approach computes AH as residual), conclusive results could not be drawn with respect to aptness of a single method. Accurate estimation of AH in urban areas can assist further in formulating policies, regulations and action plans related to mitigation and control of heat stress, climate change and improved weather forecasting.

1. Introduction

Estimation of Anthropogenic Heat (AH) in urban areas can be beneficial in understanding the modifications occurring in urban energy balance system. Growing urbanization significantly influences urban surface energy balance and led to consumption of 40% of the total energy and contribute to 86% to 96% in the total heat emissions, buildings with residential, commercial and industrial use and

* Corresponding author.
E-mail addresses: manushibhatt1995@gmail.com (M.M. Bhatt), kshama@iirs.gov.in (K. Gupta), abhidanodia@gmail.com (A. Danodia), suryatoy37@gmail.com (S.D. Chakroborty), nrpatel@iirs.gov.in (N.R. Patel).

https://doi.org/10.1016/j.heliyon.2023.e18361
Received 13 February 2023; Received in revised form 14 July 2023; Accepted 14 July 2023
Available online 17 July 2023

transportation are the largest sources of AH in urban areas [1]. AH impacts the surface energy balance because it is related to the transfer of energy between land surface and atmosphere [2] and it is an important factor contributing to rising temperatures across the globe [3]. AH flux not only impacts the temperature, but it also results into release of air pollutants from domestic, industrial and vehicle emissions into the urban atmosphere [4]. These pollutants modify the net radiation budget and eventually warm up the ambient air. Thus, estimation of AH can prove to be helpful in quantifying the impact of human activities on the environment and in turn it can be used for addressing the rising global issues related to environmental change [5,6]. Review conducted by Chapman et al. [7] states that in spite of significant importance of AH in various urban phenomenon, it is an under-researched topic; and ignoring it could mean under-estimation of rising temperatures which may lead to poor understanding of climate change phenomenon.

Anthropogenic Heat (AH) can be accounted from the process of human metabolism and release of waste energy from transportation services, building and industries [8]. The traditional methods for AH estimation included in-situ measurement of fluxes with spectro-radiometers mostly installed at roof-tops of buildings [9]. However, due to heterogeneity in urban areas, it is not feasible to conduct such measurements at a city-scale [10,11]. The inventory approach that makes use of spatially distributed energy consumption data from buildings and transportation along with other socioeconomic data can be used for a regional level AH estimation [2,9]. However, the limitation of this approach is that it is very data-intensive and it cannot be conducted very frequently at a finer resolution. Modelling approaches like Building Energy Use Approach [12–14], Surface Urban Energy and Water Balance Scheme (SUEWS) [15], Large scale Urban Consumption of Energy (LUCY) model [16], Weather Research Forecast (WRF) Model [17–19] etc. are other alternatives adopted for studying larger areas. However, few research studies [11,20–23] have made use of Earth Observation (EO) datasets as it has a much greater potential for examining the urban energy fluxes at various spatial and temporal

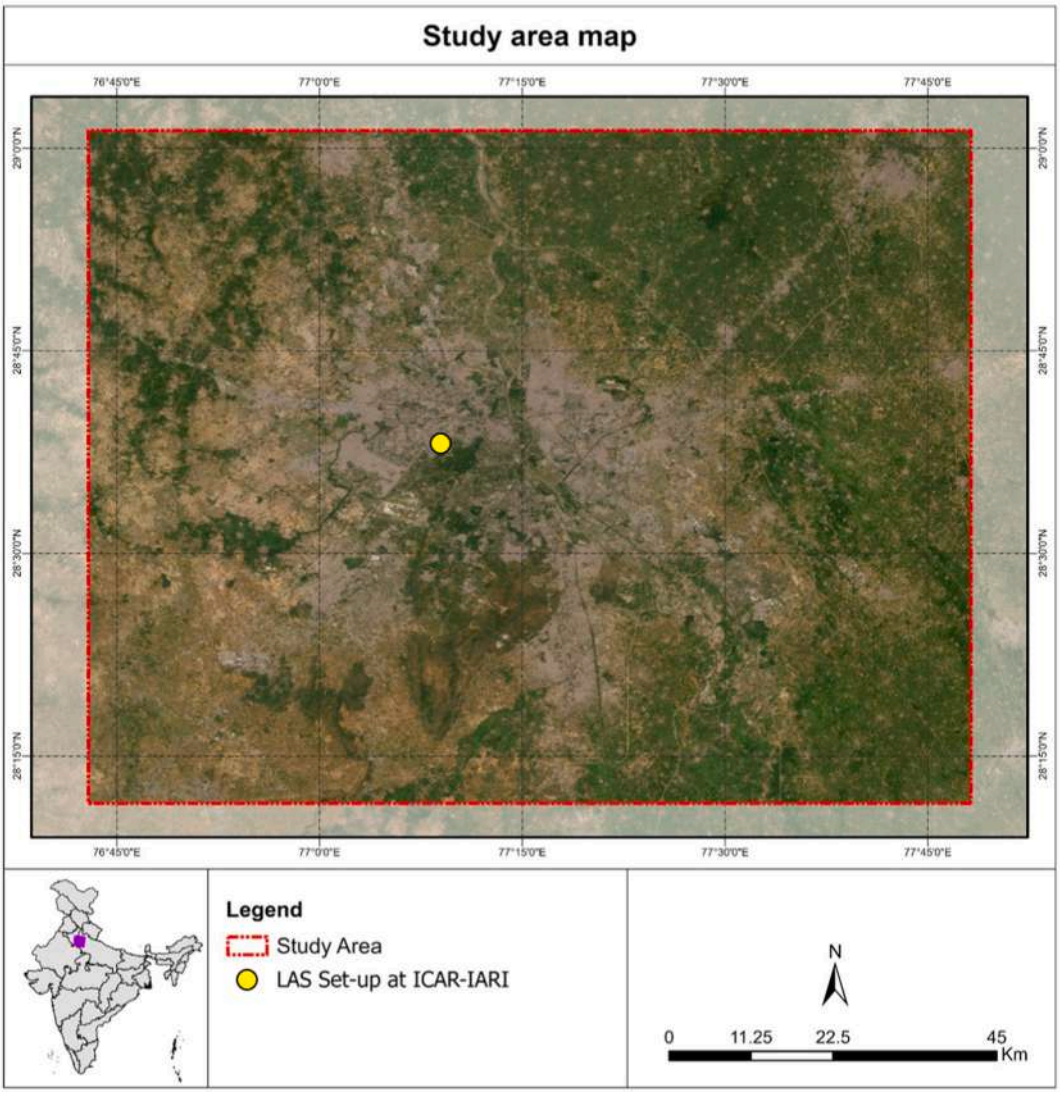

Fig. 1. Map showing the study area boundary and ground station location.

resolutions. In this approach, data from satellite images is used in a set of empirical and semi-empirical formulas to solve the energy balance equation and after placing all the flux values, AH is calculated as the residual [5,9].

There are a few studies available to derive AH from EO dataset [9,10,24] and this number is hardly a handful especially in developing region [21,23]. Kato & Yamaguchi [20] were the first ones to propose a remote sensing method that separates AH from sensible heat flux and it was applied on Nagoya city in Japan using Advanced Spaceborne Thermal Emission and Reflection Radiometer (ASTER), Enhanced Thematic Mapper Plus (ETM+) and meteorological data. Estimating AH with the help of canopy energy balance equation, ASTER data and meteorological data, research on Beijing found that AH has a role to play in the rising temperatures and urban heat island formation [9]. A spatio-temporal analysis using the Landsat data and energy balance equation showed that the magnitude of change in AH was the highest in Guangzhou city center compared to the hinterland [5]. Nitis et al. [25] calculated AH for the European cities using the ETM + dataset and the study showed that AH has a relationship with the magnitude of urbanization, economic activities and the living standards of the residents. For the Indian scenario, a study was conducted by Chakraborty et al. [21] over Delhi using Landsat and Moderate Resolution Imaging Spectroradiometer (MODIS) satellite datasets. It was observed that the area under settlement doubled over a decade from 2000 to 2010 while the increase in AH over the same was 2.5 times during winter and $\cong$ 2 times during the summer season. Another study over English Bazar Town in West Bengal, India using Landsat dataset concluded that from the year 1990 to 2017, AH increased more than 5 times against an increase of 1.5 times in the area of impervious surfaces [23].

Amongst the different factors used in AH estimation, the calculation of aerodynamic resistance is the most difficult as it depends on highly variable spatial parameters i.e. urban roughness and displacement height. However, its estimation for urban areas is very complex and methods to estimate surface roughness and displacement height in detail are lesser researched for urban areas as compared to vegetation and agricultural land [11]. It can be seen from literature that most of the studies use constant roughness value (single roughness values for entire urban area or entire Land Use Land Cover (LULC) class), which is not the case in real context as cities have varying roughness depending upon the density, height and spacing of its roughness elements. Zhang et al. [11] stated that the non-uniform height of buildings in cities makes it difficult to precisely define urban roughness height; and furthermore, urban roughness calculation error is one of the errors that has a major influence on the over/under estimation of latent and sensible heat fluxes [11,26]. Globally, only a handful of studies are available which employs detailed urban roughness characteristics for computation of urban energy fluxes whether it is a developed or developing region and none of the study has utilized detailed urban roughness characteristics for estimation of AH especially in the context of India. Besides, Authors' team computed urban roughness characteristics using low cost widely available EO based very high resolution optical stereo data, which is an innovative approach for computation of detailed urban roughness characteristics [27]. Thus, this study attempts to address the research gap of not having many studies related to estimation of AH using detailed urban surface roughness parameterization especially in the Indian context. The hypothesis framed for the study is that usage of detailed urban roughness parameters improves the accuracy of AH estimation. Based on this, the following research questions were framed for this study: (1) How EO data can be utilized for estimating urban energy fluxes? and (2) What impact does the detailed urban roughness parameter values have on the calculation of the urban energy fluxes? (3) What are the uncertainties, challenges and limitations in the estimation of AH from EO data?

2. Study area and datasets

2.1. Study area

The National Capital Territory (NCT) of Delhi and its surrounding region, an area of ~9,800 sq. km (Fig. 1) has been selected for conducting this research. It forms an interstate urban agglomeration that includes NCT of Delhi along with NOIDA and Ghaziabad in Uttar Pradesh state and Gurgaon and Faridabad in Haryana state. The population of this second largest urban agglomeration in India has increased by 21.6% from the year 2001 to 2011 [28,29]. The growth of population in surrounding towns is much higher up to 260% in just one decade of 2001–2011. Increasing population leads to enhanced usage as well as release of energy resulting into rising AH. Furthermore, the statistics from the transport department show that the rate of increase in vehicle ownership in Delhi is more than twice the rate of population growth. It is well known that vehicle emissions are the second highest contributor in the AH generation [2]. Therefore, high population density in the city, high growth rate of population and rapid increase in vehicle ownership make this region highly susceptible to concentrated AH. Chakraborty et al. [21] researched that during the year 2000 to 2010, the area under industrial land use increased by 13% while the natural land cover like open scrub, open spaces and water reduced by 10.5%, 4.6% and 0.38% respectively. Such major LULC transformations along with increasing population led to amplification of Land Surface Temperature (LST) and urban energy fluxes in the study region.

The study area falls under two climate zones Köppen climate classification Cwa which is mostly monsoon influenced humid subtropical climate and Köppen climate classification BSh which is semi-arid mostly. Delhi is landlocked with proximity to the Himalayas in the northeast and the Thar Desert in the southwest due to which it experiences both extreme winters and extreme summers. Winters span from November to February peaking in January. The temperature drops down as low as 2° Celsius during December and January. Sun is often seen in the afternoon in winters as fog and mist cover the city in the mornings. Rainy winters are also observed which benefit the Rabi crops. The weather turns warmer by March and the month of April marks the start of summer. Till the month of June, summers are observed with temperature extremes of 45° to 46° Celsius. Hot and dry winds called the 'loo' originating from the desert blow during this time to this region. The region observes monsoon due to the moisture filled southwestern winds from the Arabian Sea. The duration of monsoon is generally from the end of June to September and the region receives 80% of its annual rainfall during this period. The average annual rainfall received by Delhi is approximately 714 mm [30].

2.2. Datasets and material

Landsat 8 Operational Land Imager (OLI) and the Thermal Infrared Sensor (TIRS) tiles for (i) October 6, 2017 and October 15, 2017, (ii) March 8, 2018 and March 31, 2018 and (iii) June 3, 2018 and June 12, 2018 have been utilized in the calculation of fluxes using the EO data based approach (Table 1). This set of two tiles for one month have been used in the study as the entire study area was not covered in a single tile of same date. However, it is to be noted here that keeping into consideration the dynamic nature of various input parameters that are time sensitive, all the tiles for different dates have been processed separately.

Parameters like air temperature, dewpoint temperature, U-component of wind and V-component of wind used in various steps for flux calculation have been obtained from ERA5-Land hourly data available at the spatial resolution of $0.1^\circ \times 0.1^\circ$. ERA5 stands for European Centre for Medium-Range Weather Forecasts (ECMWF) Reanalysis data 5th generation and it is a product offered by the Copernicus Climate Change Service (C3S) at ECMWF. This atmospheric reanalysis dataset of ERA5 has a global coverage and it is available from 1950 to present date. Apart from the above listed datasets, various data/values from literature have also been used in the calculations as summarized in Table 1.

Aerodynamic resistance values used for calculating the sensible heat flux and latent heat flux have been calculated using three distinct approaches. First approach uses a constant roughness value for entire study area (referred herein as Method −1), second approach uses Land Use Land cover obtained using Landsat 8 OLI and values form literature for calculation of roughness values (referred herein as Method −2) following the approach of Hu et al. [9] while third approach uses pixel by pixel varying Zom values (detailed urban roughness parameterization) obtained from Very High Resolution Satellite (VHRS) optical stereo data (Pleiades Panchromatic (PAN) and Multispectral (MX) of 0.5 m resolution and 2 m resolution respectively) for calculation of roughness and zero plane displacement height (referred herein as Method-3) (Table 1).

In-situ observations of net radiation values from the Automatic Weather Station (AWS), sensible heat flux values from the Large Aperture Scintillometer (LAS) and ground heat flux values from soil heat flux plate were compared with the fluxes estimated using EO-based approach for each of the six Landsat tiles. Each of the above listed instruments are located in the premises of ICAR-IARI, Pusa campus, New Delhi. Further details regarding ground observations have been provided in section 3.5.

Table 1
Dataset used in the study.

Parameters derived	Sensor	Date	Spatial Resolution	Purpose
NDVI	Landsat 8 OLI	October 6, 2017	30 m	Surface Emissivity & Ground Heat Flux
LULC		October 15, 2017		R_{smin}, & z_{om}
Albedo		March 8, 2018		Net radiation & Ground Heat Flux
Incoming Shortwave Radiation		March 31, 2018		Net radiation
Surface Emissivity		June 3, 2018		Net radiation and LST
		June 12, 2018		
Land surface temperature	Landsat 8 TIR	October 6, 2017	30 m	Net radiation, Ground Heat Flux, Sensible Heat Flux, and Stomatal Resistance
		October 15, 2017		
		March 8, 2018		
		March 31, 2018		
		June 3, 2018		
		June 12, 2018		
Incoming Longwave Radiation	ERA5-Land hourly data	October 6, 2017	$0.1^\circ \times 0.1^\circ$; Native resolution 9 km	Net radiation
Air temperature		October 15, 2017		Incoming longwave radiation, Sensible Heat Flux, Latent Heat Flux
Dewpoint temperature		March 8, 2018		Actual vapor pressure
Wind speed		March 31, 2018		Sensible Heat Flux and aerodynamic resistance
Saturated vapor pressure		June 3, 2018		Latent Heat Flux estimation
Actual vapor pressure		June 12, 2018 (6:00 UTC)		Latent Heat Flux estimation
Roughness parameters	Literature			Sensible and Latent Heat Flux estimation
	Very high resolution PAN & multispectral optical satellite stereo (Pleiades)	2012 to 2017 (14 Scenes)	0.5 m and 2 m	
Stomatal resistance	Literature, Shortwave Radiation and LST			Latent Heat Flux
Flux observations	Ground observations from Large Aperture Scintillometer (LAS), ICAR-IARI, Pusa campus, New Delhi			Validation and Comparative evaluation of three approaches used for roughness calculation

3. Methodology

3.1. Study design

Owing to the availability of detailed urban surface roughness parameters for the year 2017 and in-situ measurement data for validation for 2017 and 2018, the present study was conducted for October 2017, March 2018 and June 2018 to test the aptness and uncertainty of the proposed methods.

Surface Energy Balance (SEB) Model has been employed for computation of AH, whereas set of equations are employed to compute the Net Radiation (Rn), Ground Heat Flux (G), Sensible Heat Flux (H) and Latent Heat Flux (LE). AH has been calculated as the residual of SEB model (Equation (19)). All the urban energy fluxes have been calculated using three different methods based on difference in parameterization of urban roughness as explained in Section 2.2. Rn and G values derived for each of the three methods will be the same as there is no change in the variables used to derive these fluxes across the three methods. Employing the set of equations explained in Section 3.4.1 and 3.4.2, net radiation and ground heat flux were derived using Landsat 8 optical and thermal data along with ERA5 Land hourly data.

Then, the sensible heat flux and latent heat flux were estimated by employing three methods as explained earlier. It is to be noted here that the equations used across the three methods are the same (Section 3.3) but the only difference lies in the estimation and use of urban surface roughness values (Zom). Method 1 uses a single Zom value across the entire study area, Method 2 uses Zom values referred from the literature and a single value being assigned to the entire LULC class and Method 3 uses pixel by pixel varying Zom

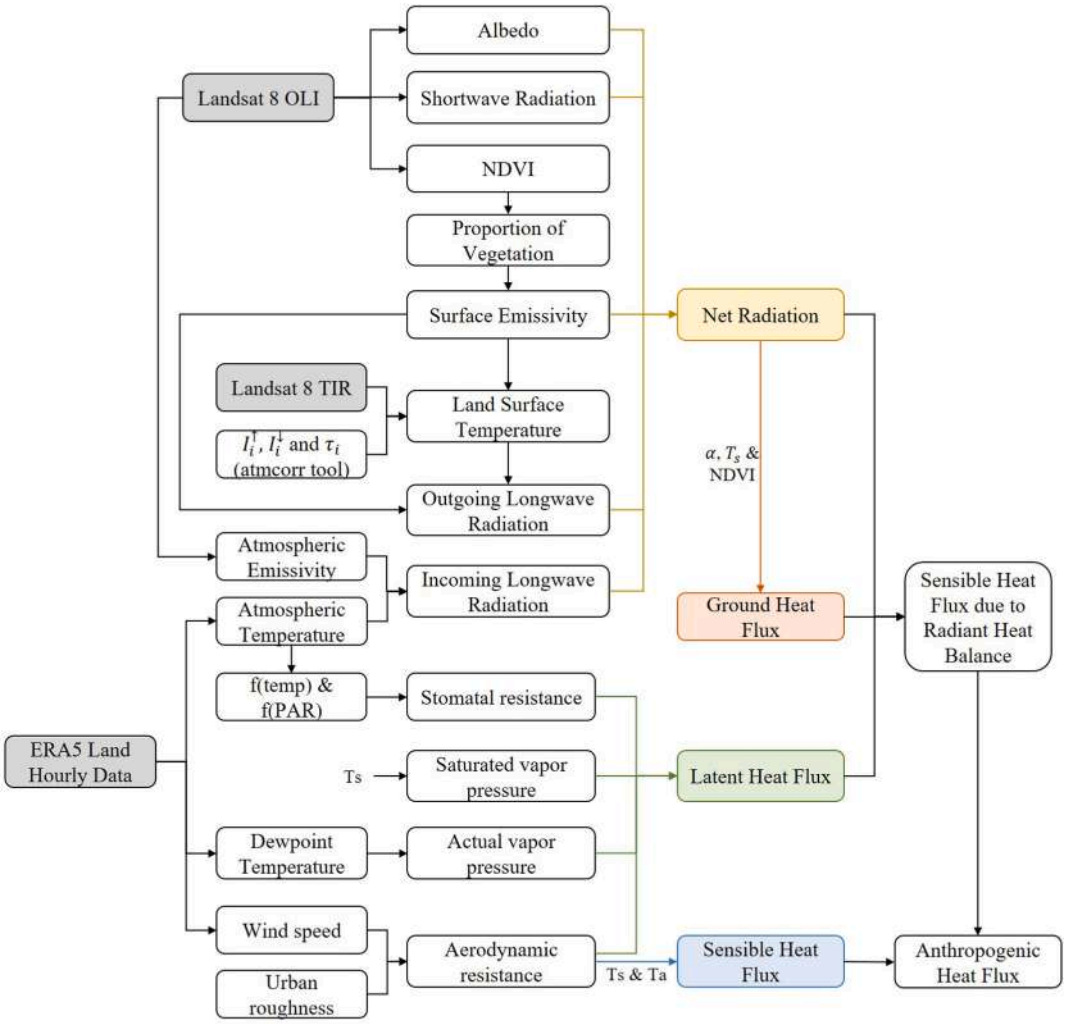

Fig. 2. Methodology adopted to estimate anthropogenic heat flux in the present study.

values (detailed urban roughness parameterization). Other parameters used in sensible and latent heat flux estimation have been derived using Landsat 8 optical plus thermal data, ERA5 Land hourly data and literature. Lastly, the AH values obtained from all the three methods were validated with the ground data and a comparative analysis of the same was conducted (Fig. 2).

3.2. LULC classification

Supervised classification using Maximum Likelihood Classification (MLC) method was performed on Landsat 8 image tiles of 6th October and October 15, 2017. For classifying the image, a minimum of 10n (n = number of Landsat bands used for classification) training samples were taken and the land use land cover classification of the study area has been done into 5 broad categories namely (i) Waterbodies, (ii) Vegetation and Dense Agriculture, (iii) Agriculture and Urban Parks, (iv) Built-up and (v) Bare soil. Further, accuracy assessment of the classified mosaicked image was done by generating 50 ground truth points per LULC class with equalized stratified random sampling method. Finally, an error matrix with overall accuracy and kappa co-efficient was generated based on the classified values vs ground truth values.

3.3. Urban roughness

The urban fabric in cities is the roughest surface form [31]. The buildings are impermeable, hard and inflexible as compared to the vegetation due to which they reduce the wind flow causing surface drag [4]. Urban surface roughness is defined based on a set of parameters related to the urban morphology like zero plane displacement, roughness length, frontal area density, building plan area fraction, height to width ratio etc. and these can be estimated using morphometric or micrometeorological approaches. Urban roughness (z_{om}) is an important parameter for sensible and latent heat flux calculation and has an impact on accuracy of AH estimation.

Method-1 applies a single value of urban roughness values (z_{0m}) estimated using Equation (1) [31] for the entire study area. In the equation below, h represents average obstacle height (in meters) and f_0 is empirical constant value.

$$z_{0m} = f_0 h = 0.10\ h\# \tag{1}$$

Method-2 uses typical z_{om} values adopted from the study by Kato & Yamaguchi [26] for each LULC class (Table 2).

Detailed spatially variable surface roughness values, used in the present study for Method-3 has been derived as part of long term research conducted by the Authors' team [27]. VHRS Optical Stereo Panchromatic (PAN) and Multi-spectral data of Pleiades 1A/1B satellite were employed to extract Digital Surface Model (DSM) and Digital Terrain Model (DTM). The normalized DSM (nDSM) was eventually derived as nDSM = DSM – DTM. Building heights from nDSM and building footprint area extracted from LULC classification were used to quantify building surface fraction. Building volume and mean building height were calculated to further compute volumetric averaged building height (h_{vk}) using building footprints and nDSM. Zero plane displacement was estimated using building surface fraction and volumetric averaged building height (h_{vk}). It is to be noted here that application of freely available Urban Multi-scale Environmental Predictor (UMEP) tool [32] in the study area could not provide satisfactory results for the computation of roughness characteristics in the dense and complex urban environment of study area [33] and Urban Morphology Extractor (UME) tool, developed by the authors' team [33], were employed to compute Frontal area index (λ_f) [33], which is further employed for computation of z_{om} in the study area. Mathematically, the area of vertical wall surface in a specific wind direction divided by the unit horizontal surface area gives frontal area index. Finally using all the above calculations, detailed surface roughness (z_{om}) values were estimated for Delhi by employing the morphometric approach (Equation (2)) [34].

$$z_{om} = (h_{vk} - Z_d) exp\left(- \frac{k}{\sqrt{0.5 \lambda_f C_{dh}}} \right) \# \tag{2}$$

Where h_{vk} is volumetric averaged building height, Z_d is zero plane displacement height, k is Von Karman's constant (k = 0.4), λ_f is frontal area index in a particular wind direction and C_{dh} is drag coefficient dependent on obstacle shape.

3.4. Energy balance equation

The energy balance equation is usually represented as shown in Equation (3) [15].

Table 2
Accuracy assessment results, surface roughness values (z_{om}) and minimum resistance values (r_{smin}) for each LULC class.

Sr no.	LULC type	Accuracy		z_{0m} value	r_{sMIN} values
1	Water	95.24%		0.00003	0
2	Vegetation	83.33%		0.5	60
3	Agriculture	83.33%		0.1	90
4	Built-up	92.86%		1.5	–
5	Bare soil	92.85%		0.001	500
		Overall Accuracy	**91.27%**		
		Kappa	**0.90**		

$$R_n = G + LE + H\# \tag{3}$$

Where, R_n is net radiation, G is ground heat, LE is latent heat and H is sensible heat fluxes. But in urban areas, apart from the natural heat the anthropogenic activities (A) also add on to the energy balance. So, Equation (4) represents the urban energy balance equation. The present study estimates anthropogenic heat (AH) as the residual of the urban energy balance equation [15].

$$R_n + AH = G + LE + H\# \tag{4}$$

Where, R_n is net radiation, G is ground heat, LE is latent heat, H is sensible heat fluxes and AH is Anthropogenic Heat.

3.4.1. Net radiation

Net radiation is the balance of the addition of net longwave radiation and net shortwave radiation (Equation (5)) and it has been estimated as [9,15].

$$R_n = (1-\alpha)R_{S\downarrow} + R_{L\downarrow} - R_{L\uparrow} - (1-\varepsilon_o)R_{L\downarrow}\# \tag{5}$$

Where, R_n is net radiation, α is albedo, $R_{s\downarrow}$ is incoming shortwave radiation, $R_{L\downarrow}$ is incoming longwave radiation, $R_{L\uparrow}$ is outgoing longwave radiation and ε_o is surface emissivity.

In this study, surface albedo has been calculated using the formula given by Waters et al. [35] and the equation requires top of atmosphere albedo (α_{TOA}) which was calculated using the equation adopted by Beg et al. [36].

Here, Surface albedo has been calculated using SEBAL formula [35].

$$\alpha = \frac{\alpha_{TOA} - \alpha_{path_{radiance}}}{{\tau_{sw}}^2}\# \tag{6}$$

In Equation (6), $\alpha_{path\_radiance}$ is the average of incoming solar radiation across all the bands that is back-scattered to the satellite before it reaches the surface of the earth. Its value has been taken as 0.03 [35]. The top of atmosphere albedo (α_{TOA}) was calculated using Equation (7) [36] and τ_{sw} is transmissivity.

$$\alpha_{TOA} = 0.356ref_2 + 0.326ref_3 + 0.138ref_4 + 0.084ref_5 + 0.056ref_6 + 0.041ref_7 \ \# \tag{7}$$

Here, ref_i is the reflectance values of the respective band.

Shortwave radiation, incoming longwave radiation and outgoing longwave radiation have been estimated with the set of formulas given by Waters et al. [35]. Surface emissivity has been estimated using the Normalized Difference Vegetation Index (NDVI)-based emissivity method (NBEM) by following the approach employed by Nikam et al. [37].

To derive the above-mentioned parameters, there is a requirement to input air temperature (T_a) and Land surface temperature (T_s) values in the equations. Therefore, the values of air temperature were retrieved from the 2 m Temperature dataset of ERA-5 Land hourly data while the LST for the study area was calculated by applying the Radiative Transfer Equation (RTE) on Landsat-8 thermal dataset. Landsat-8 has two thermal bands capturing data in the wavelength region of 10.60 to 12.51 μm and these bands can be utilized for application of Split-Window (SW) algorithm for land surface temperature retrieval. However, application of SW algorithm has a few limitations in estimating water vapor content and land surface emissivity because the universal parameters applicable to the SW algorithm are not yet available for Landsat-8 [37] and besides it is observed that RTE method using single TIR band provide accurate results better than SW algorithm [38]. It has also been observed that the accuracy of band 11 in Landsat-8 is dubious due to the stray light problem and so, usage of band 10 for LST calculation is more preferable [39]. Therefore, in this study band 10 has been used for land surface temperature estimation using RTE. The atmospheric correction parameters required in the equation including up-welling path radiance ($I_i^{\uparrow},$), down-welling path radiance ($I_i^{\downarrow}$) and atmospheric transmittance (τ_i) have been extracted from the online 'Atmospheric Correction Parameter Calculator' that uses National Centers for Environmental Prediction (NCEP) data.

3.4.2. Ground heat flux

Ground heat flux (G) has been estimated using Equation (8) [35].

$$\frac{G}{R_n} = \frac{T_s}{\alpha}\left(0.0038\alpha + 0.0074\alpha^2\right)\left(1 - 0.98NDVI^4\right)\# \tag{8}$$

Where, R_n is the net radiation, T_s is the land surface temperature and α is albedo (same as derived for net radiation [36]).

3.4.3. Sensible heat flux

Sensible heat flux has been calculated using Equation (9) and Equation (10) [35].

$$H = \frac{\rho C_p dT}{r_a}\# \tag{9}$$

$$dT = T_s - T_a\# \tag{10}$$

In the above equations, ρ is the air density (1.2 kg/m^3), C_p is the specific heat of air at constant pressure (1005 J/kg K) and dT is the

temperature difference between the land surface temperature (T_s) and atmospheric temperature (T_a). r_a which is the aerodynamic resistance has been estimated with the formula given in Equation (11).

$$r_a = \frac{\ln\left(\frac{z_2}{z_1}\right)}{u_* k} \# \tag{11}$$

Here, z_1 and z_2 are the minimum and maximum heights respectively of the built-up in the study area. Then, k is von Karman's constant (0.41) and u_* is the friction velocity (in m/s). The value of u_* is computed using Equation (12) [15,25].

$$u_* = \frac{k\, u_x}{\ln\left(\frac{z_x}{z_{om}}\right)} \# \tag{12}$$

The friction velocity is calculated using the values of known wind speed (u_x) at height z_x. For the present study, ERA5 wind speed data at 10 m height has been put into equation (12) for calculation and z_{0m} is the roughness height for momentum transfer (in meters) (Section 3.2).

Unlike net radiation and ground heat flux values that are the same for all the three methods, the values for sensible heat flux and latent heat flux calculated change in each of the three methods due to distinct urban surface roughness (z_{0m}) values.

3.4.4. *Latent heat flux*

Latent heat flux has been calculated using Equation (13) [26].

$$LE = \frac{\rho C_p \left(e_s^* - e_a\right)}{\gamma (r_a + r_s)} \# \tag{13}$$

In the above equation, ρ is the air density (1.2 kg/m^3), C_p is the specific heat of air at constant pressure (1005 J/kg K), γ is the psychrometric constant (0.67 hPa/K), e_s^* is saturated vapor pressure, e_a is actual vapor pressure, r_a is aerodynamic resistance and r_s is stomatal resistance. e_s^* and e_a have been calculated using Equation (14) and Equation (15) respectively [40]. The dewpoint temperature (T_{dew}) used in the following Equation (15) has been retrieved from ERA5-Land hourly data.

$$e_s^* = 0.6108 * \exp\left[\frac{17.27 * T_s}{T_s + 237.3}\right] \# \tag{14}$$

$$e_a = 0.6108 * \exp\left[\frac{17.27 * T_{dew}}{T_{dew} + 237.3}\right] \# \tag{15}$$

Nishida et al. [41] has given a modified formula for calculating r_s using only remote sensing parameters and the same formula has been used in this study (Equation (16)).

$$\frac{1}{r_s} = \frac{f_1(T_a)\, f_2(PAR)}{r_{sMIN}} + \frac{1}{r_{cuticle}} \# \tag{16}$$

Here, r_{sMIN} is the minimum resistance and the values for the same have been taken based on land use land cover category as listed in Table 2 [26].

And, $f_1(T_a)$ and $f_2(PAR)$ in Equation (16) are the functions of temperature and photosynthetic active radiation (PAR) respectively that can be estimated using the following set of formulas (Equation (17), Equation (18) and Equation (19)).

$$f_1(T_a) = \left(\frac{T_a - T_n}{T_o - T_n}\right) \left(\frac{T_x - T_a}{T_x - T_o}\right)^{\left(\frac{T_x - T_o}{T_o - T_n}\right)} \# \tag{17}$$

$$f_2(PAR) = \frac{PAR}{PAR + A} \# \tag{18}$$

$$PAR = R_s * 2.05 \# \tag{19}$$

Table 3
Parameters for calculating r_s.

Parameter	Value
Cuticle resistance ($r_{cuticle}$)	100,000 sm^{-1}
Minimum temperature for stomatal activity (T_n)	2.7 °C
Maximum temperature for stomatal activity (T_x)	45.3 °C
Optimal temperature for stomatal activity (T_o)	31.1 °C
Photon absorption efficiency (A)	152 °C

The values of certain parameters for estimation of $f_1(T_a)$ and $f_2(PAR)$ have been taken from the study conducted by Nishida et al. [41] (Table 3).

3.4.5. Anthropogenic heat flux

From radiant heat balance, the sensible heat can be calculated as shown in Equation (20) [21].

$$H_n = R_n - G - LE\# \tag{20}$$

And finally the sensible heat flux due to anthropogenic effects (H_{as}) can be expressed as shown in Equation (21). In case the value of H is smaller than that of H_n in Equation (21), H can be replaced with H_n to solve the formula [13].

$$H_{as} = H - H_n\# \tag{21}$$

3.5. Validation of urban energy fluxes

It can be inferred from the literature review that validation is one of the most popular approaches of uncertainty assessment in EO data based methods [42] and therefore, the present study uses in-situ measurements of net radiation, sensible heat flux and ground heat flux for validation. The comparative evaluation of surface energy fluxes was done using the Large Aperture Scintillometer (LAS)

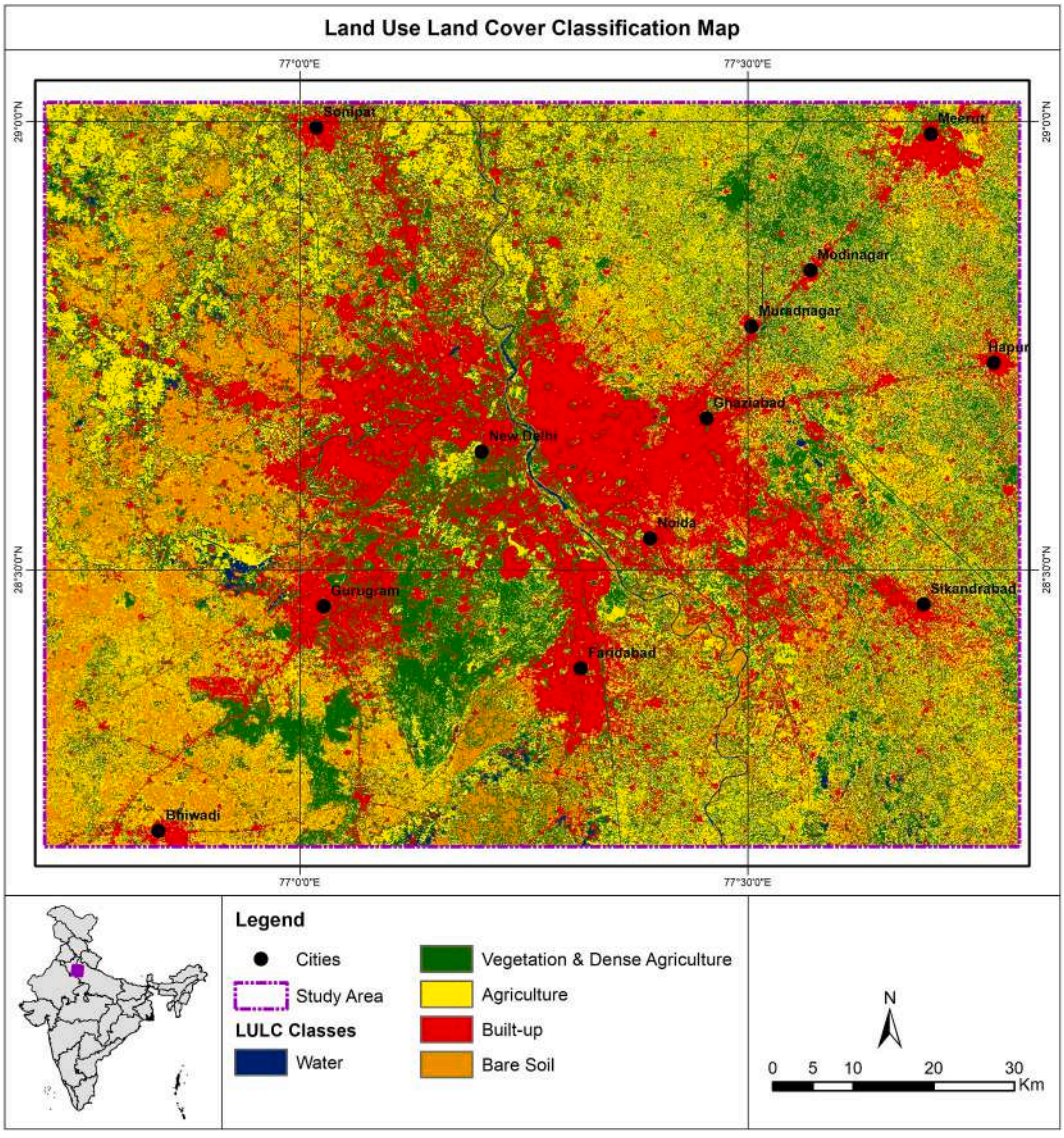

Fig. 3. Land use land cover map.

Table 4
LULC class wise analysis of mean flux values for each method.

		October 2017				March 2018				June 2018			
		Vegetation	Agriculture	Built-up	Bare Soil	Vegetation	Agriculture	Built-up	Bare Soil	Vegetation	Agriculture	Built-up	Bare Soil
Rn (in W/m2)		505.34	477.34	461.50	422.47	470.18	458.35	449.86	425.74	428.92	409.99	404.15	383.83
G (in W/m2)		72.33	69.97	77.40	77.10	65.51	63.24	67.05	64.64	78.46	77.77	78.80	76.82
H (in W/m2)	Method 1	25.79	37.65	42.28	73.53	44.79	51.47	50.81	67.89	−198.14	−124.08	−68.04	−75.08
	Method 2	15.29	14.51	36.46	22.12	25.81	20.54	45.44	18.93	−99.44	−43.24	−71.32	−25.01
	Method 3	4.72	10.40	44.83	38.33	31.38	31.16	74.08	60.98	−165.92	−77.17	−72.27	−65.96
LE (in W/m2)	Method 1	303.19	262.76	23.81	105.76	261.62	212.25	9.56	78.88	869.99	601.11	33.49	183.69
	Method 2	214.22	152.91	16.59	68.57	183.58	121.99	6.53	50.84	767.19	502.91	29.36	160.05
	Method 3	283.09	208.28	22.38	85.44	222.11	160.38	10.78	70.07	812.68	545.24	38.83	172.64
Has (in W/m2)	Method 1	104.03	106.95	318.00	166.08	98.26	131.39	322.44	214.32	−321.39	−144.81	359.91	198.41
	Method 2	203.50	239.94	331.04	254.69	195.28	252.58	330.84	291.33	−321.33	−129.71	368.57	180.22
	Method 3	120.36	172.20	306.71	212.03	151.18	203.57	298.35	230.04	−299.87	−137.77	359.16	208.58

set-up which is installed in the premises of ICAR-IARI, Pusa campus, New Delhi. This set-up of LAS has transmitter and receiver end which are at the distance of 990 m for the detailed observations of surface energy fluxes. LAS set-up is one of the kind of high end sensing instrumentation which measure the sensible heat flux at 5 min interval and its functioning is based on the principle of Monin-Obhukov Similarity Theory (MOST). This set-up also comprises Automatic Weather Station (AWS) for measurement of net radiation by net radiometer and soil heat flux by soil heat flux plate. This entire set-up provided the observations of the all components of surface energy fluxes. This entire path length of the instrumentation is located over an irrigated agricultural landscape. The maize and wheat are the predominant crops during Kharif (Mid-June to October) and Rabi (Mid-November to April). Thus, there are more

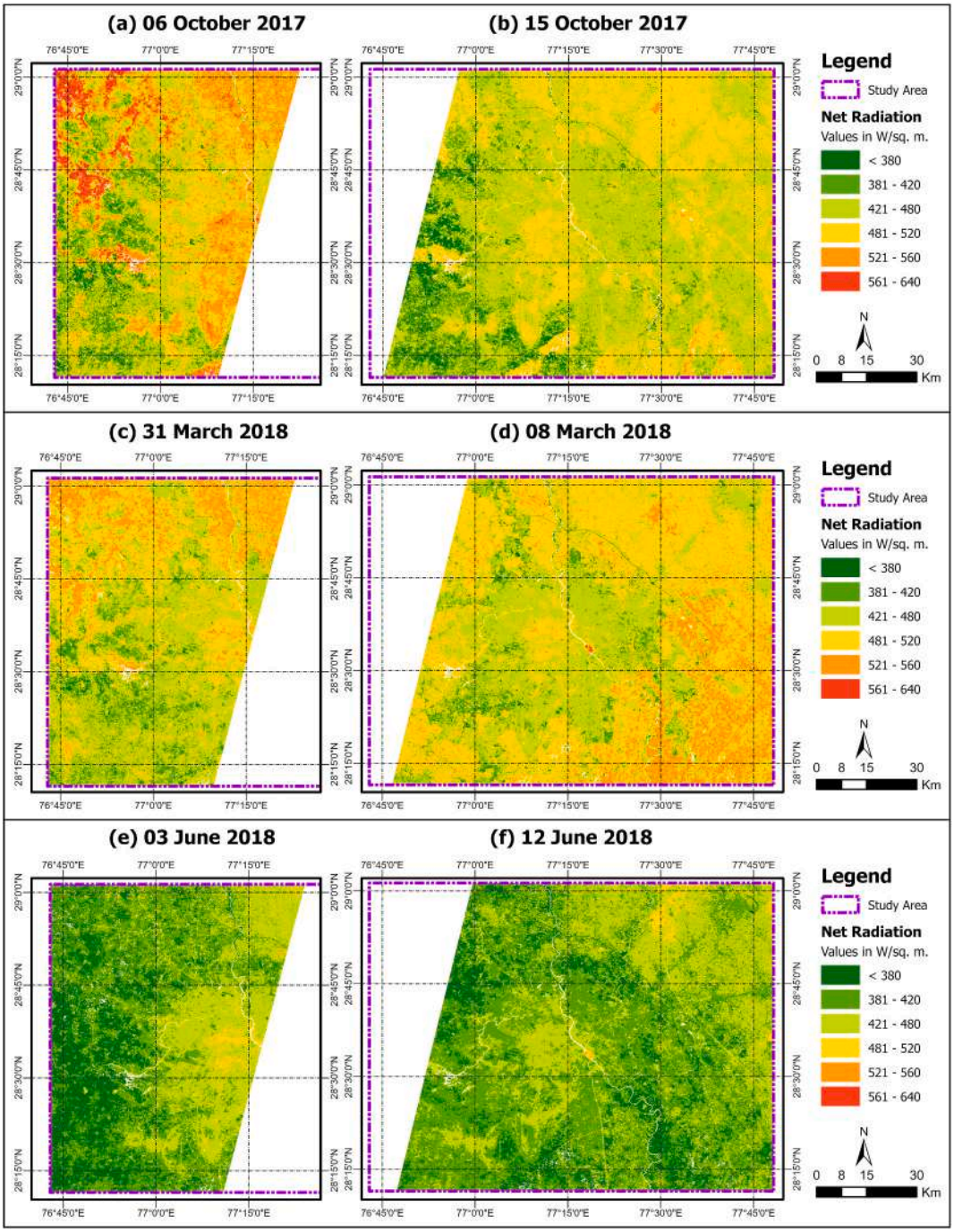

Fig. 4. Net radiation map for (a) October 6, 2017 (b) October 15, 2017 (c) March 31, 2018 (d) March 8, 2018 (e) June 3, 2018 and (f) June 12, 2018.

agricultural/crop fraction in October and March months while June depicts the fallow or bare land parcel observations. The campus being located within the city area is surrounded by mostly built-up. The data retrieved from LAS set-up has been used for comparative analysis of the estimated fluxes.

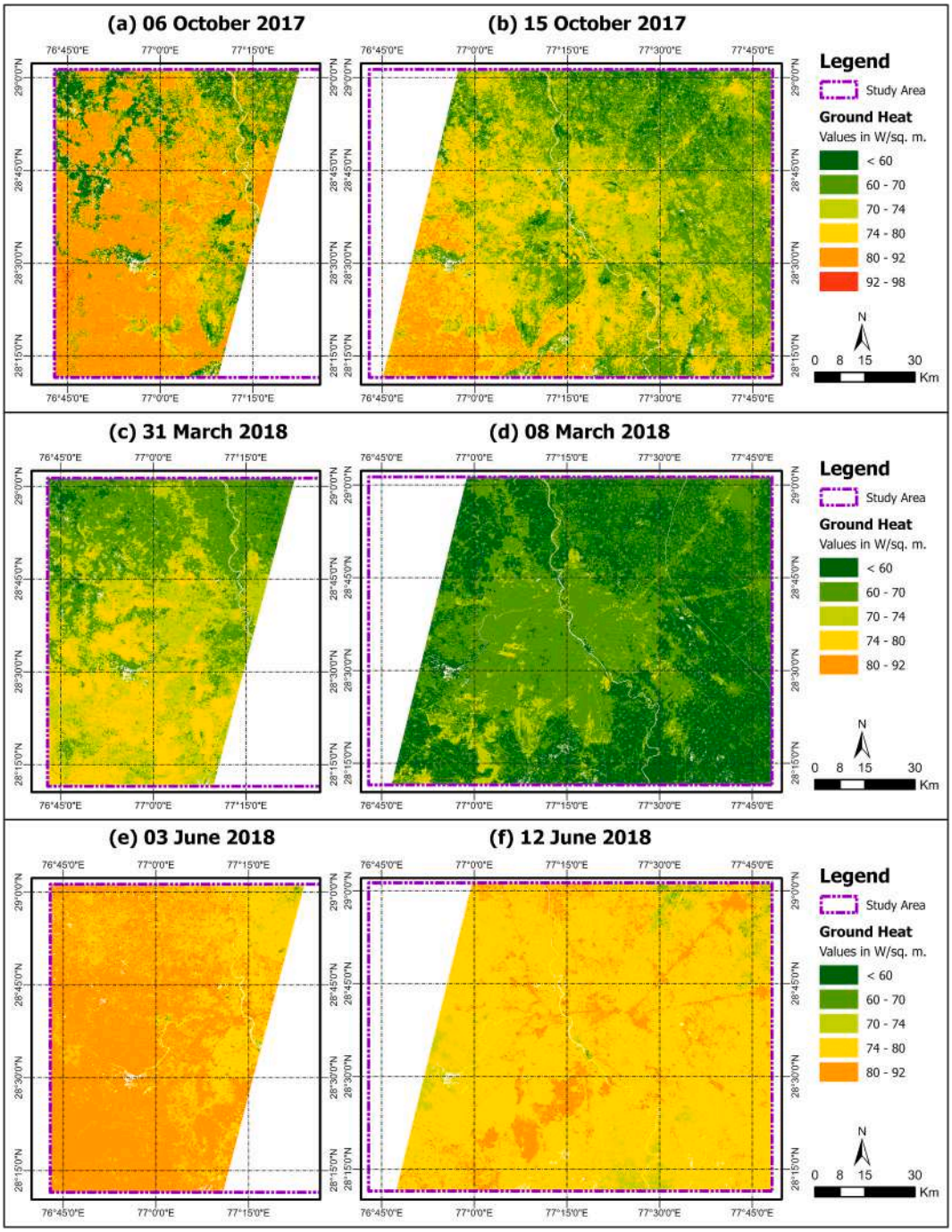

Fig. 5. Ground heat flux map for (a) October 6, 2017 (b) October 15, 2017 (c) March 31, 2018 (d) March 8, 2018 (e) June 3, 2018 and (f) June 12, 2018.

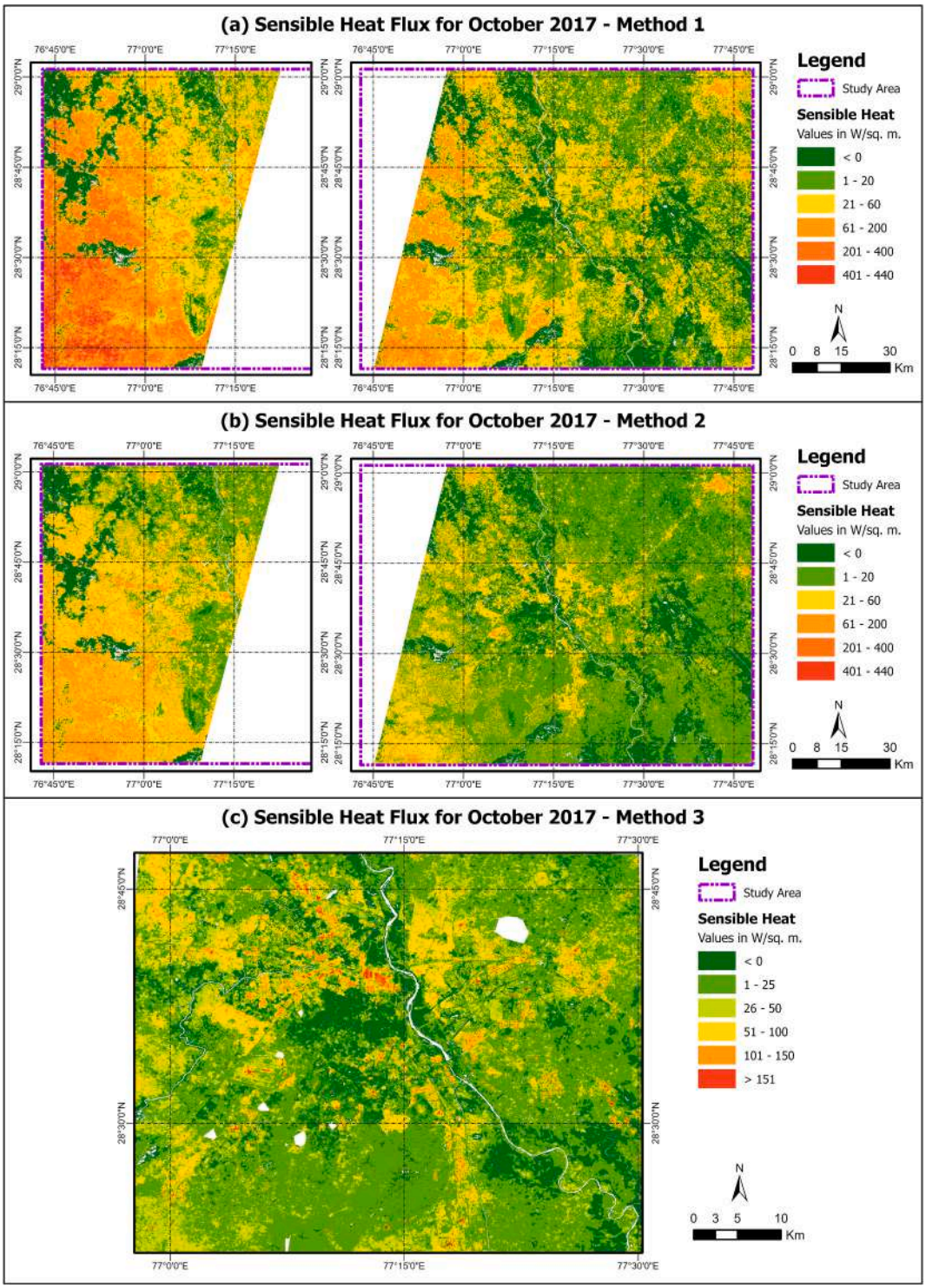

Fig. 6. Sensible Heat Flux for 6th and October 15, 2017 obtained using (a) Method 1 (constant Zom) (b) Method 2 (LULC-based Zom) (c) Method 3 (Detailed Zom).

4. Results

4.1. Input parameters for energy balance approach

The LULC classification (Fig. 3) shows the built-up of Delhi being extracted in the central part of the image followed by Gurugram to the southwest, Noida and Faridabad in the southeast and Ghaziabad to the east. Other cities, towns and village cores are also classified into built-up while the Malcha forest and Asola forest to the south are classified into vegetated areas. The rest of the study area is either agriculture or bare soil. The overall accuracy of the MLC based LULC classification is found to be 91.27% with a kappa co-efficient of 0.90 (Table 2).

4.2. Net radiation

Vegetation class is observed to have the maximum net radiation in all the three months (505.34, 470.18 and 428.92 W/m^2 for October 2017, March 2018 and June 2018 respectively) followed by agriculture class (477.34, 458.35 and 409.99 W/m^2 for October 2017, March 2018 and June 2018 respectively), built-up (461.5, 449.86 and 404.15 W/m^2 for October 2017, March 2018 and June 2018 respectively) and bare soil (422.47, 425.92 and 383.83 W/m^2 for October 2017, March 2018 and June 2018 respectively) in a decreasing order of values (Table 4). Urban settlement or built-up in the center of the study area is seen to have comparatively lower net radiation than the agricultural land and vegetation in all the three seasons because the nature of storing heat is not at its peak at the time of satellite pass that is around 10:54 a.m. (Fig. 4 (a)-(f)). Overall, the highest net radiation is observed in the month of October while the least is noted for all the LULC classes during June which is the pre-monsoon shower period.

4.3. Ground heat flux

Built-up is observed to have the highest average ground heat flux amongst all the LULC classes with values of 77.40, 67.05 and 78.80 W/m^2 for October 2017, March 2018 and June 2018 respectively and amongst the three time periods, it is the highest for June 2018 (Fig. 5 (a)–(f) and Table 4). The difference between the ground heat flux values of different LULC classes is higher in October 2017 and it is the least for June 2018 (Table 4). The same is visually discernible from Fig. 5 as well where the distinction between LULC classes is visible for October 2017 with bare soil having highest ground heat flux while on the other hand, urban areas and its adjoining areas both have high ground heat flux. However, a comparison between the three time periods shows that ground heat flux values of all the LULC classes are the least in the month of March as compared to June and October months which are the pre-monsoon and post-monsoon time periods respectively.

4.4. Sensible heat flux

Sensible heat flux values obtained using the first method results into bare soil LULC class having the highest values of 73.53 and 67.89 W/m2 for October 2017 (Fig. 6a) and March 2018 respectively. However, using the second method, sensible heat flux values for built-up class is the highest with values 36.46 and 45.44 W/m2 for October 2017 (Fig. 6b) and March 2018 respectively. The same trend of built-up class having the highest sensible heat flux values is seen in method 3 as well with sensible heat flux values of 44.83 and 74.08 W/m2 for October 2017 (Fig. 6c) and March 2018 respectively.

Sensible heat flux values for all the LULC classes obtained using method 2 are lower in comparison to method 1 in general. Whereas, method 3 shows lower sensible heat flux values all three LULC classes except built-up class as compared to method 1 (Table 4). However, the overall sensible heat flux values of all the LULC classes derived using method 3 lies in between the range of values obtained from method 1 and method 2 in case of March 2018 and June 2018 but for October 2017, these values obtained in method 3 are least amongst the three methods.

Built-up class being highest in method 1 and bare soil class being highest in method 2 and 3 amongst all LULC classes is true in case of sensible heat flux for June 2018 as well. But the only difference is that the sensible heat flux values for all the classes are in negative which denotes energy transfer from surface to atmosphere. The possible reason for the same can be that it is the time just before the rainy season starts in the study area so the ground is cooling and water vapor condensation occurs.

A comparison between the three time periods i.e. October 2017, March 2018 and June 2018 shows that the sensible heat flux for all the LULC classes show a trend where values are highest during March followed by October month and the values are noted to be in negative for the month of June. Thus, it can be observed that pre-monsoon shower period observes least sensible heat flux in the Delhi region and this is true for results obtained from all the three methods.

Sensible heat flux values are highest for first method and least for the second method for all the three time periods and the values obtained through the third method with detailed urban roughness values lies in between the two for the three time periods. However, a comparison between the average sensible heat flux values of different LULC classes show that there is a maximum difference in between the LULC classes in method 3 followed by method 1 and method 2 respectively. The same can be interpreted from Fig. 6 (a), Fig. 6 (b) and Fig. 6c where method 3 shows more spatial segregation of flux values across the LULC classes because of inclusion of detailed urban roughness. In October 2017 and March 2018 results, the dense urban built-up, industries and market along the railway line in the northwest part of Delhi can be identified with higher sensible heat flux. The airport building is visible in dark red showcasing high sensible heat flux. The compact built-up near the river on the east and towards the farther western end is seen to have moderate sensible heat flux values. On the other hand, the central part of the city with dense trees is found to have the least sensible heat flux and

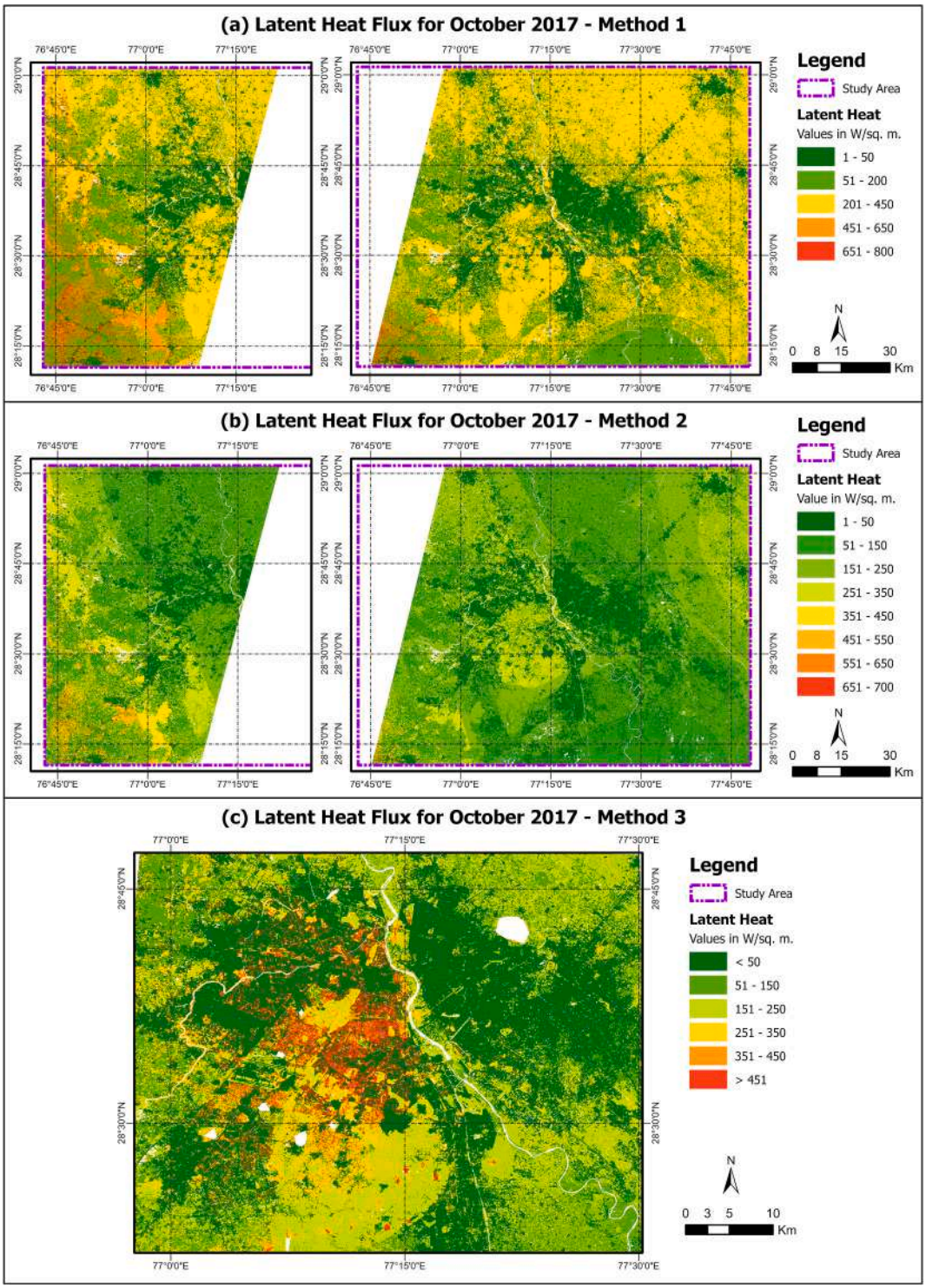

Fig. 7. Latent Heat Flux for 6th and October 15, 2017 obtained using (a) Method 1 (constant Zom) (b) Method 2 (LULC-based Zom) (c) Method 3 (Detailed Zom).

the forest ranges to the south of the city are identified with low sensible heat flux (Fig. 6).

4.5. Latent heat flux

Latent heat flux shows nearly opposite trend and pattern as compared to sensible heat flux as generally observed by other researchers as well. Vegetation and agriculture have higher latent heat flux than the bare soil class and built-up class (Fig. 7 a, b and c). The highest latent heat flux values are noted for vegetation class using all the three methods in all the three time periods (Table 4). June 2018 is noted to have highest latent heat flux for vegetation class amongst the three time periods using all the three methods (869.99 W/m^2 for method 1, 767.19 W/m^2 for method 2 and 812.68 W/m^2 for method 3). Agriculture class observes the second highest latent heat flux values for all the three time periods and in all the three methods. Amongst the LULC classes, built-up class is noted to have the least latent heat flux values for all the three time periods. A seasonal comparison of the latent heat flux values for built-up class shows that the month of March has the least values (9.56 W/m^2 for method 1, 6.53 W/m^2 for method 2 and 10.78 W/m^2 for method 3) as compared to the June (monsoon) and October (post-monsoon) time periods. However, it should be noted that unlike certain studies that assume the latent heat flux to be zero for urban areas [20], this study has considered the fact that urban green spaces and vegetation within the extent of urban area influence the estimation of heat fluxes in built-up area.

A comparison between the latent heat flux values obtained using the three different methods, the values derived using method 1 is the highest while that derived using method 2 are the least. The range of flux values obtained using detailed urban roughness

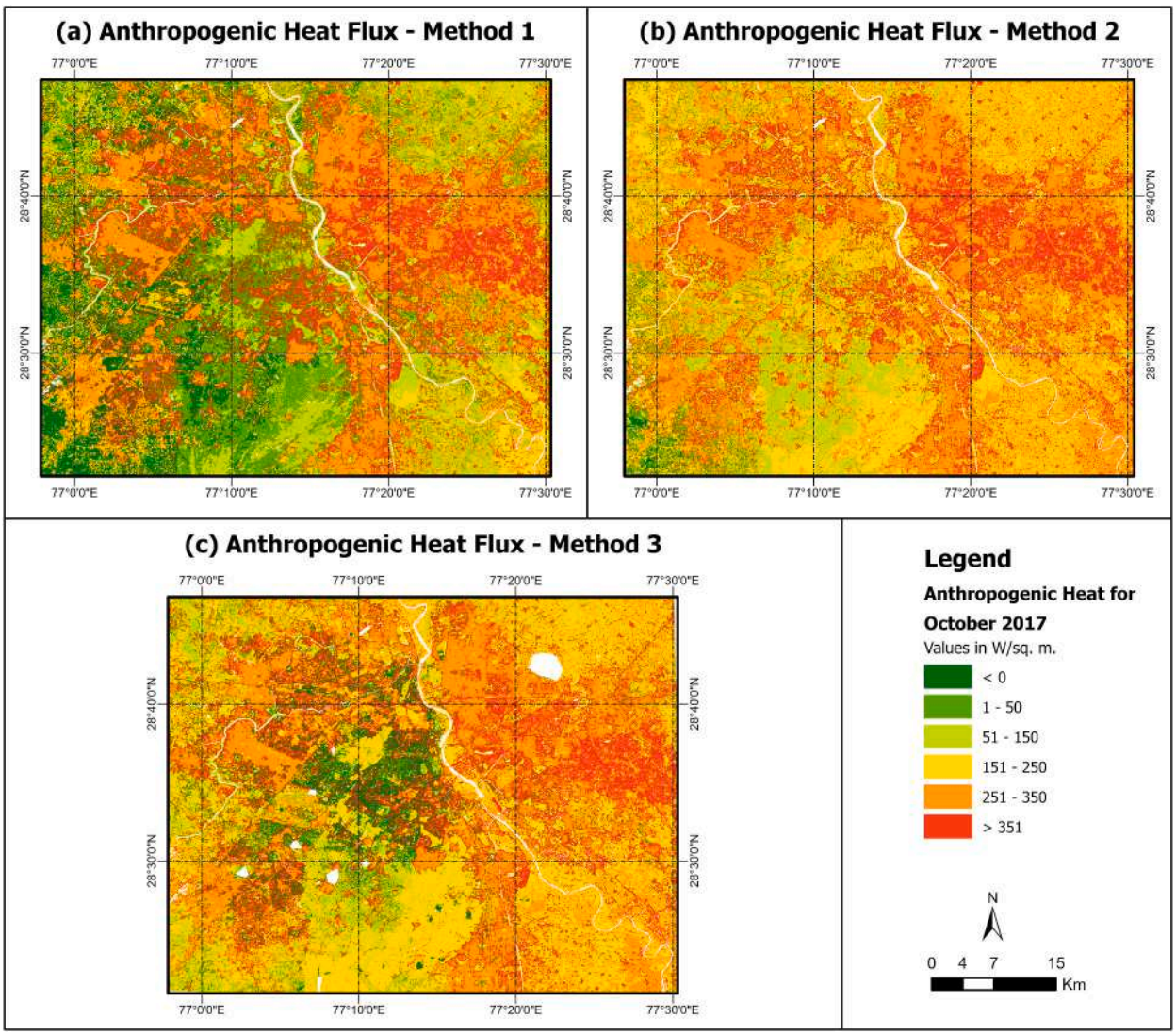

Fig. 8. Anthropogenic Heat Flux for October 2017 obtained using (a) Method 1 (constant Zom) (b) Method 2 (LULC-based Zom) (c) Method 3 (Detailed Zom).

parameterization in method 3 lie in between the other two methods.

4.6. Anthropogenic heat flux

Amongst all the LULC classes, built-up class observes the highest AH values in all the three time periods and this is true in case of AH values obtained using all the three methods (Table 4). Out of the three time periods, June 2018 has the highest AH values for built-up class (359.91 W/m^2 for method 1, 368.57 W/m^2 for method 2 and 359.16 W/m^2 for method 3). Out of the three methods, method 2 is observed to have the highest AH values while method 3 has the least AH values for all the three time periods (Table 4).

In October 2017, built-up areas have AH values greater than 250 W/m^2 for method 1 (Fig. 8a), method 2 (Fig. 8b) and method 3 (Fig. 8c). The average AH values estimated for October 2017 are 318 W/m^2 using method 1, 331.04 W/m^2 using method 2 and 306.71 W/m^2 using method 3 respectively. In March 2018, majority of the built-up areas can be seen to have AH values in range of 250 to 350 W/m^2 in all the three methods (Fig. 9a, b and c) but the proportion of areas having AH greater than 350 W/m^2 is the least in method 3 (Fig. 9c) and highest in method 2 (Fig. 9b). As compared to the other two time periods where most of the built-up observed AH values within the range of 250 to 350 W/m^2, most of the built-up in June 2018 has AH greater than 350 W/m^2.

AH values obtained using method 2 for the rest of non-built-up classes like vegetation, agriculture and bare soil shows that there is an overestimation as compared to method 1 and 3 for October 2017 and March 2018 time periods. This can be easily visualized from Fig. 8 for October 2017 and Fig. 9 for March 2018 where clear distinction between the urban core vs. surrounding LULC classes is not as

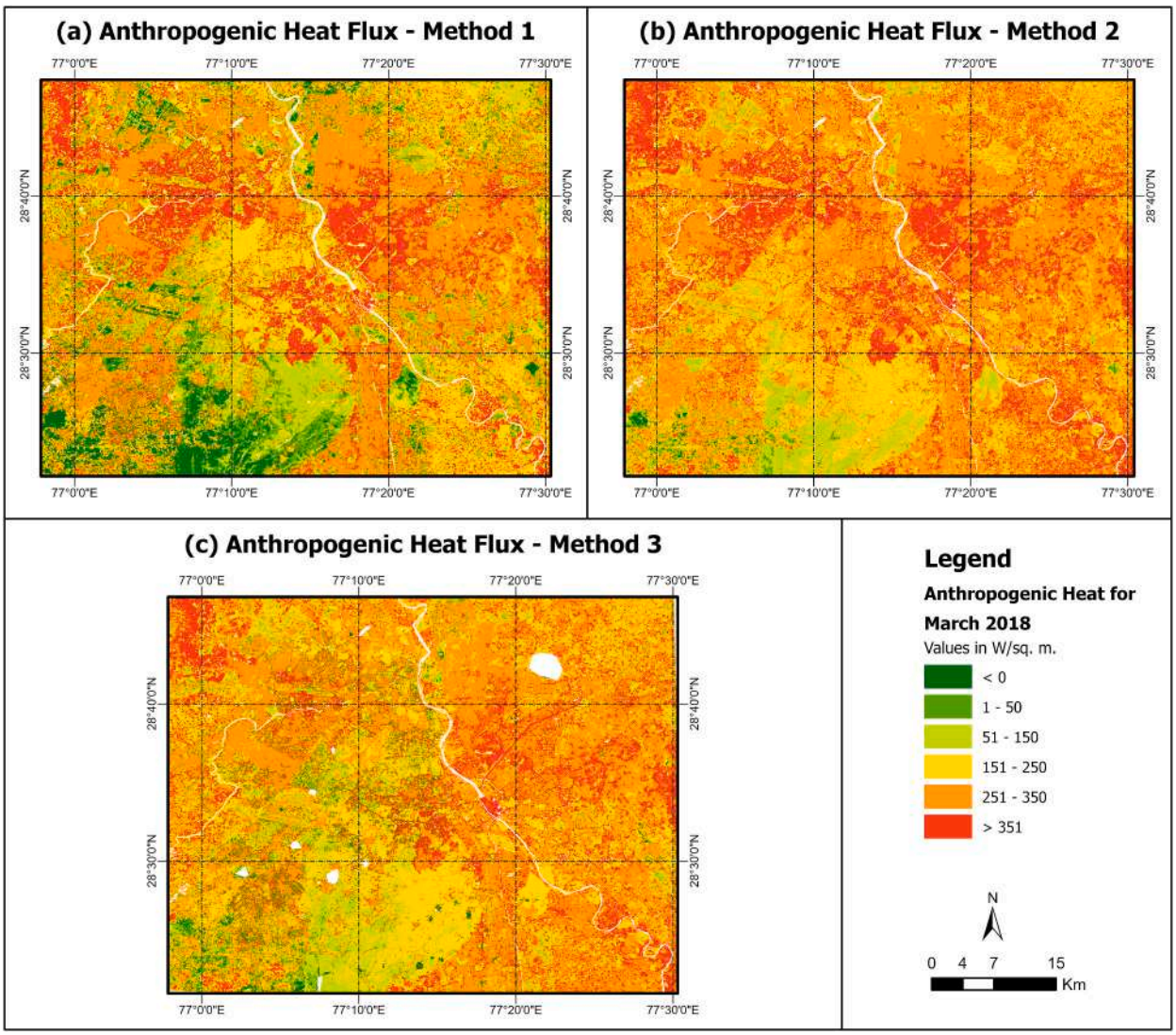

Fig. 9. Anthropogenic Heat Flux for March 2018 obtained using (a) Method 1 (constant Zom) (b) Method 2 (LULC-based Zom) (c) Method 3 (Detailed Zom).

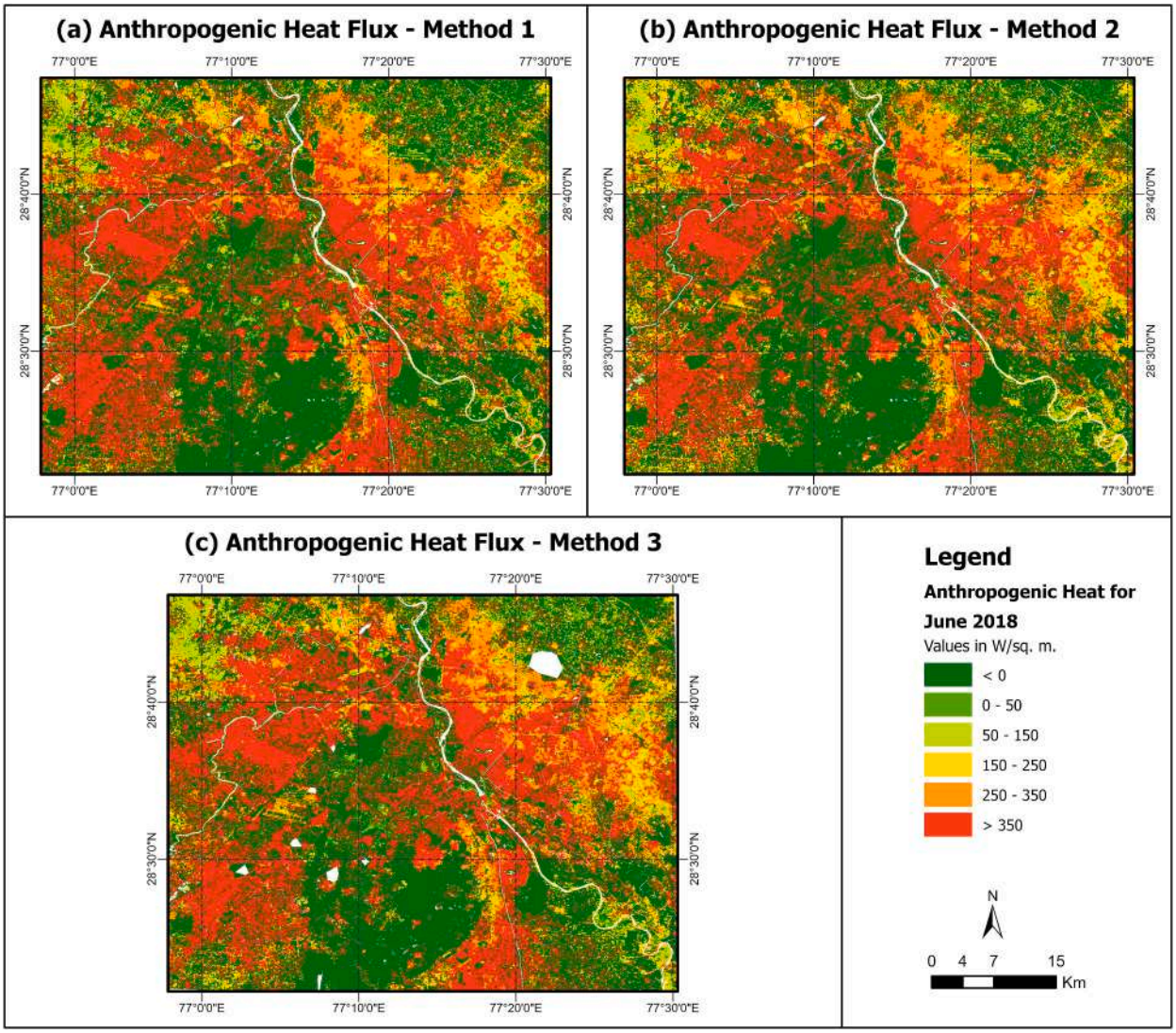

Fig. 10. Anthropogenic Heat Flux for June 2018 obtained using (a) Method 1 (constant Zom) (b) Method 2 (LULC-based Zom) (c) Method 3 (Detailed Zom).

sharp as the one seen for method 1 and method 3. However, this trend is not seen in case of June 2018 and there is a sharp distinction between the built-up vs non-built-up classes in all the three methods (Fig. 10 (a)-(c)). Unlike October 2017 and March 2018, in June 2018 all the non-built-up classes shows negative AH values estimated using each of the three methods.

Spatial distribution of AH for the Method 3 is found to be the best for all the three time periods (Figs. 8–10). The use of detailed urban roughness layer in the third method results into better spatial representation of AH values which is otherwise not discernible in rest of the methods. A clear depiction of roads and paved surfaces with high anthropogenic heat values is seen. Urban green spaces in the neighborhoods can be observed to have lower AH value. The central part of Delhi near Connaught place has the least AH values due to the presence of dense trees. The newly developing areas of Noida in the southeast and that of Gurugram in the southwest can be seen to have the highest AH due to the presence of a lot of high-rise structures in that areas. The densely built neighborhoods in the northern part of Faridabad and certain industrial areas have AH value crossing the mark of 350 W/m^2 in all the three time periods. Also, the average AH values calculated in this method for all the LULC classes are not as high as the second method.

4.7. Validation with ground observations

In-situ measurements of net radiation, sensible heat flux, ground heat flux and latent heat flux from LAS set-up at IARI campus were retrieved for all the three time periods and compared with the results obtained from each of the three methods. It is to be noted that net radiation and ground heat flux values are the same for all the three methods while the calculation of sensible and latent heat flux varies

as per the level of detailing in urban roughness values. A comparison of flux values for all the six tiles (2 tiles representing one-time period of that respective month) has been done with the in-situ measurement at the respective satellite overpass time.

Net radiation flux values estimated from EO data based approach are in close correspondence with in-situ measurements for almost all the tiles with a mean difference between the in-situ values vs. estimated values is −16.17 W/m^2 except one tile in March where EO data overestimated the net radiation with a value of −154.55 W/m^2 (Table 6). There is an overestimation of net radiation values for October 2017 and March 2018 while the values are underestimated for June 2018 in the EO data based approach as compared to the in-situ measurements.

The estimated ground heat flux values of 78.73 and 76.95 W/m^2 for 6th and October 15, 2017 respectively has a larger variation from the LAS set-up in-situ measurement value of 12.43 W/m^2. A similar overestimation of 40.9 and 42.47 W/m^2 has been observed for 3rd and June 12, 2018 respectively (Table 6). While the least difference between in-situ measurement and EO data based approach can be noted for March 8, 2018 (21.16 W/m^2) and March 31, 2018 (21.27 W/m^2).

Sensible heat flux values obtained from all three methods shows close correspondence to the in-situ measurement values except in case of June 2018. The sensible heat flux at ground observation site is 66.80 W/m^2 while sensible flux obtained from all three methods ranges from 54.45 to 60.99 W/m^2 for October 2017. However, the method-3 which uses detailed urban roughness parameterization (sensible flux value of 60.99 W/m^2) is the closest to the field observation (66.80 W/m^2) for October 2017. Method-1 with single roughness value for the entire study area (sensible heat flux of 60.24 W/m^2) also shows close correspondence with ground data as compared to the second method which uses roughness value from the literature as per the LULC classes. In case of March 2018, the sensible heat flux values for method 2 has least difference between in-situ measurement and EO data based approach (−6.46 and −13.11 W/m^2 for March 8, 2018 and March 31, 2018 respectively). While June month shows large overestimation of 106.25 W/m^2 for June 3, 2018 and an underestimation of 195.14 W/m^2 for June 12, 2018 (Table 6).

Validation of latent heat flux and AH could not be carried out as LAS setup do not provide observations on these two fluxes. Besides, comparative assessment of the flux values for each LULC class cannot also be carried out as LULC class-wise in-situ measurement was not available.

5. Discussion

5.1. Estimation of urban energy fluxes

The present study demonstrates successfully the potential of EO data for estimation of spatial distribution of AH and surface energy fluxes in an Indian urban area i.e. Delhi region. The availability of information on AH from EO data in this region is crucial as urban areas in this region experience high urban growth and pollution levels due to increasing population pressure and density. The study has large potential to be replicated globally especially in the countries of developing region such as Asia, Africa and Latin America having similarities to the study area where paucity of detailed inventory on population, transportation and industrial activities limits the use the inventory based approaches at finer scales for estimation of AH.

The study also demonstrates the impact of detailed urban roughness parameterization obtained using VHRS Optical stereo on the estimation of surface urban energy fluxes which resulted in better spatial distribution of all surface energy fluxes especially AH. It is also noted that estimation of urban fluxes using constant roughness value for entire urban area also provide reasonable results in terms of spatial distribution.

The close correspondence of net radiation observed through AWS and estimated from EO data for most of the dates highlights the potential of EO data for estimation of urban surface energy fluxes at high resolution. A comparison of the mean estimated albedo values and mean emissivity values from EO data based approach also shows close corroboration with the values found in literature. The calculated mean values of albedo and emissivity for all the LULC classes fall within the ranges defined by Oke et al. [4] in his study (Table 5).

AH estimated in this study (mean AH value of 318.33 W/m^2 for October 2017, 317.21 W/m^2 for March 2018 and 362.55 W/m^2 for June 2018) shows close correspondence with the studies conducted earlier in Delhi region [21] for a time period of 2000 to 2010 which showed an increase in anthropogenic heat values from 158.01 to 217.77 W/m^2.

5.2. Bowen ratio

In most of the studies, Bowen ratio which is the ratio of sensible heat flux to latent heat flux is used for comparison as it is difficult to

Table 5
Comparison of Albedo and surface emissivity.

LULC Class	Mean Albedo in study area	Albedo range from study by Oke et al. (2017)	Mean surface emissivity in study area	Surface emissivity range from study by Oke et al. (2017)
Vegetation and dense agriculture	0.19	0.16 to 0.26 (low vegetation) 0.13 to 0.20 (decidous forests)	0.978	0.90 to 0.98 (low vegetation) 0.90 to 0.99 (decidous forests)
Agriculture	0.20	0.18 to 0.25 (crops)	0.974	0.90 to 0.99 (crops)
Built-up	0.22	0.09 to 0.23 (Urban) 0.11 to 0.24 (Sub-urban)	0.980	0.94 to 0.96 (Urban & Sub-urban)
Bare Soil	0.24	0.18 to 0.30 (light color dry soil)	0.978	0.89 to 0.98 (light color dry soil)

Table 6
Comparison of Surface Energy fluxes obtained with ground observations.

	LAS Observation	Method 1	Method 2	Method 3
06-Oct-17				
Rn	436.8	479.6		
G	12.43	78.73		
H	66.8	60.24	54.45	60.99
Residual	357.57	340.63	346.42	339.88
15-Oct-17				
Rn	323.90	400.51		
G	17.09	76.95		
H	83.39	88.65	16.50	44.62
Residual	223.42	234.91	307.06	278.94
08-Mar-18				
Rn	267.70	422.25		
G	44.68	65.84		
H	42.01	48.47	40.75	33.77
Residual	181.02	307.94	315.66	322.64
31-Mar-18				
Rn	400.10	444.35		
G	50.68	71.95		
H	121.41	134.52	121.59	158.60
Residual	228.01	237.88	250.81	213.80
03-Jun-18				
Rn	447.00	386.69		
G	40.33	81.23		
H	170.00	276.25	249.70	222.95
Residual	236.67	29.21	55.76	82.51
12-Jun-18				
Rn	407.25	384.75		
G	36.67	79.14		
H	251.45	56.31	50.89	50.73
Residual	119.13	249.29	254.71	254.87

compare absolute flux values across cities as the fluxes vary greatly according to location and time of the study. Amongst the three methods, method 2 gives the highest Bowen ratio for all the three time periods, followed by method 3 and lastly, method 1. The Bowen ratio observed over the study area in October 2017 is 1.99, 2.19 and 2.00 using method 1, 2 and 3 respectively and 2.03, 2.42 and 1.86 for June 2018 using method 1, 2 and 3 respectively which is close to the ratio value of 2.55 for Basel city [4]. The predominant built-up characteristic of Basel city is compact mid-rise, which resembles to that of Delhi. However, a comparison of Bowen ratio obtained for March 2018 is approximately 6 which is close to the value reported for Vancouver (5.42) [4]. The reason for an increased Bowen ratio in March is due to decreased latent heat flux during that season.

5.3. Challenges, uncertainties and limitation in measurement of fluxes from EO data

Moderate to large deviation from ground based observations in estimation of ground heat flux and sensible heat flux from EO data is may be due to the difference in measurement approach in both the techniques. The ground instrument measures net radiation, ground heat flux and sensible heat flux which is put into the energy balance equation to obtain latent heat flux as the residual. It does not take into consideration AH separately while solving the energy balance equation unlike the way it is done in EO data based approach. Therefore, the in-situ measurement values of the fluxes might have AH component into any or all of the fluxes due to which the estimated flux values might not exactly match the ground observed flux values. Hence, one to one comparison of both techniques for all fluxes except net radiation may not yield conclusive results. However, since no other ground observations was available, it is being used in this study for validation of obtained results. More number of observations over varying land cover and urban densities may assist to validate the results in much better way in future. Besides, ground heat flux depends on the type of land cover, water content in the soil and net radiation. The location of the field instrument (Fig. 1) is such that the nearby land is constantly irrigated for conducting agricultural studies due to which the ground heat flux of the immediate surrounding at the given time can be noted to be low or underestimated.

One of the main reasons of variation between the in-situ measurement and EO data based approach might be due to difference in footprint of both estimations. The observations taken from the LAS set-up are point data with a path length of 990 m that are being compared with a pixel of 30 m. The set-up being in the city area, there is a mixing of varied land use inside the 30 m pixel which is being measured with the flux value at a single point, a limitation reported by earlier studies as well. Additionally, it should be noted that the flux observations recorded by LAS set-up are at a 5-min interval which is not available for the exact time of satellite overpass for comparison with flux values estimated using the EO data based approach. Therefore, an average of the recorded in-situ flux values from the two nearby time intervals has been used in the study for validation.

The distribution of LST significantly impacts the computation of sensible heat flux and subsequently the computation of AH. It can be observed that bare soil shows highest mean LST, while mean LST of built-up class does not show significant variation with respect to

vegetation and agriculture class. The possible reason for this phenomenon is that Delhi region tend to show 'Urban Cool Island Effect' during the early half of the day [43,44] due to the presence of mostly arid and semi-arid natural cover. So, at the time of satellite pass i.e. around 10:55 a.m., the LST noted from the built-up area in the urban core is lesser than that of the bare soil and fallow agricultural land located in the periphery of the urban area. The net radiation of the built-up as well is seen to be falling within moderate range because the nature of storing heat is not at its peak during the time at the time of satellite pass. Besides, LST being one of the important parameter for computation of surface fluxes, uncertainties in LST estimation arising due to estimation of land surface emissivity, atmospheric vapor content, sensor viewing angle, heterogeneous land surfaces etc. may also propagate in the estimation of surface energy fluxes.

Another limitation of the study is that uncertainty in any of the key input parameters in the study like air temperature, land surface temperature, incoming shortwave and longwave radiations wind speed etc. can propagate to final energy flux estimations. Since, AH is calculated as the residual of the energy balance equation therefore, any error caused in estimating the rest of the fluxes will account into underestimation or overestimation of AH. In future, a sensitivity analysis of all the input parameters may assist in determination of parameters which has significant effect on estimation of various fluxes and furthermore, estimation of AH. Besides, there is an assumption made in the EO data based approaches using the energy balance equation that the phenomenon of advection is not taken into account considering its negligible effect.

Due to non-availability of meteorological datasets for the study area, parameters like air temperature, dewpoint temperature, U-component of wind and V-component of wind used in various steps for latent and sensible heat flux calculation have been obtained from ERA5-Land hourly data. But this dataset is available at a very coarse spatial resolution of $0.1^{\circ} \times 0.1^{\circ}$ which might cause uncertainty in calculation of fluxes. Lastly, the detailing of roughness parameters has been limited to mainly urban areas and that is also for one-time period only. However, roughness values especially for vegetation areas may vary from season to season and might have an impact on estimation of sensible and latest heat fluxes which in turn may have an impact on estimation of AH. Therefore, seasonally varying availability of roughness especially for agriculture and vegetation area in future might lead to improved AH estimation.

AH values for October 2017, March 2018 and June 2018 are observed to be the highest using Method-2 as compared to the rest of the two methods. The possible reason for the same can be that the Zom values in this method have been inferred from the literature which is mostly available for developed countries in Mediterranean climate and a single value for the entire LULC class has been assigned. Nevertheless, availability of LULC-wise roughness values in Indian or similar climate regions in the future may improve the result obtained from this method as well.

AH values obtained for agriculture and vegetation classes also show positive values in October 2017 and March 2018. This might be attributed to the limitation faced in performing detailed LULC classification, significant transportation and human activities due to dense population in surrounding areas and proximity to the megacity. Besides, the study region has a presence of thousands of brick kiln in and its close surroundings in the periphery of the urban core which might have been classified into agriculture and bare soil due to which the mean AH for these classes is also showing high values. However, in absence of detailed spatial data it is difficult to determine exact number of brick kilns in selected study area. Uncertainty in calculating sensible heat flux and latent heat flux due to any one of the input parameters as discussed earlier might also affect the estimation of AH which is computed as residual of SEB equation.

Waste heat from residential areas, commercial areas, industries and transportation services contribute to the anthropogenic heat [45]. But the limitation of EO-data based approach is that it cannot account for details like building energy emissions and vehicular emissions separately because the set of equations used to derive urban energy fluxes in EO-data based approach do not use such details for input. For such a detailed approach of AH estimation, inventory approaches or building energy use approaches can be used if energy consumption-emission data of buildings, industries, transportation and human metabolism can be gathered. At present, such detailed datasets are not available for Indian cities however, in future with availability of data other approaches or a combination of approaches can be applied.

6. Conclusion

EO data potential for estimation of spatial distribution of AH and surface energy fluxes is well demonstrated in this study for an Indian urban area. The study also discusses various challenges, limitations and uncertainties in computation of input parameters which impacts the estimation of AH from EO data. However, in absence of detailed inventory data at finer scales, AH from EO data is one of the best alternative as it provides better spatial distribution with high spatial resolution. Hence, study has enormous potential to be replicated in urban areas of developing region of similar characteristics which experience non-availability of detailed information on population, transportation and activities at finer scales, mandatory to use the inventory based approaches. Net radiation and sensible heat flux values estimated from EO-based approach are found to have close correspondence with ground observations of Large Aperture Scintillometer (LAS) setup for all the three methods. Additionally, the spatial distribution of surface energy fluxes and AH was found to be better in method 3 due to employment of detailed urban roughness values obtained using VHRS Optical stereo; followed by results of method 1 that uses a single urban roughness value for the entire urban area. Hence, it was concluded that the usage of roughness values estimated with fine scale urban parameterization leads to better estimation of anthropogenic heat however, in absence of such meticulous data the use of single urban roughness value is also recommended. However, due to difference in approach for estimation of fluxes (LAS setup computes latent heat flux as residual while EO based approach computes AH as residual), conclusive results could not be drawn with respect to aptness of a single method.

The present study uses Landsat 8 data for estimating AH using EO data based approach. In future, the applicability of these three methods can be checked with any other satellite offering data from which the surface energy balance equation variables can be

derived. Apart from change in datasets, in future these methods may be applied to other study regions in India to assess the uncertainty of the three methods. In this study, EO data of only instantaneous time at the satellite overpass has been employed to estimate the AH for each of the three time periods (October 2017, March 2018 and June 2018). As a future scope of research, long term trend analysis of spatio-variation in AH for day vs night, hourly variation, daily aggregates, annual trend etc. can be conducted. This may assist in better understanding of the influence of urban form and geometry on micro climatic variation, Urban Heat Island (UHI), spatial variation of temperatures and hot spots etc. in urban areas. Besides, detailed spatial information on AH can be ingested in high resolution urban weather and climate models such as Weather research and Forecasting model, Urban Canopy Models etc. for improved weather forecasts in urban areas. Methods offering improved accuracy of spatially distributed AH estimation will eventually lead to refined canopy layer and UHI modelling results and their understanding. It is expected that AH estimation will also play an important role in formulating policies, regulations and action plans to take measures for climate action.

Declarations

Availability of data and material

The results and conclusion of the study were derived from the following data sources:

(1) Landsat 8 OLI and TIRS: The data is freely available and can be obtained from USGS earth explorer website.
(2) Detailed Urban roughness derived using VHRS Optical Satellite Stereo raw data can be shared upon reasonable request case to case basis within the purview of data security policy. VHRS Optical Satellite Stereo raw data of the study region was used from the archive of the institute (Indian Institute of Remote Sensing, Dehradun) and cannot be shared openly.
(3) Ground Survey data: (a) Field Survey data that includes ground truthing data for LULC can be shared upon reasonable request. (b) Ground Observation data of Large Aperture Scintillometer (LAS) data can be shared upon reasonable request case to case within the purview of data security policy.

Author contribution statement

Manushi M. Bhatt: Performed the experiments, Analyzed and interpreted the data, Wrote the Paper; Kshama Gupta: Conceived and designed the experiments, Analyzed and interpreted the data, Wrote the Paper; Abhishek Danodia: Analyzed and interpreted the data, contributed analysis tools and data, Wrote the Paper; Surya Deb Chakraborty: Contributed analysis tools and data, Wrote the Paper; N R Patel: Contributed analysis tools and data, Wrote the Paper.

Ethics approval

The work is carried out at corresponding author's institute as part of ongoing research. The work reported is original and has not been published elsewhere, nor is it currently under consideration for publication elsewhere. All the research articles have been cited appropriately in the manuscript as per the defined style and format.

Funding statement

This research is part of an ongoing research at the institute and received no external funding to conduct the research.

Declaration of competing interest

The authors declare that they have no known competing financial interests or personal relationships that could have appeared to influence the work reported in this paper.

References

[1] Y. Wang, Y. Li, S. Di Sabatino, A. Martilli, P.W. Chan, Effects of anthropogenic heat due to air-conditioning systems on an extreme high temperature event in Hong Kong, Environ. Res. Lett. 13 (2018) (S Di Sabatino).
[2] S. Chen, D. Hu, Parameterizing anthropogenic heat flux with an energy-consumption inventory and multi-source remote sensing data, Rem. Sens. 9 (2017), https://doi.org/10.3390/rs9111165.
[3] IPCC, Climate Change 2022 Mitigation of Climate Change, 2023.
[4] T.R. Oke, G. Mills, A. Christen, J.A. Voogt, Urban Climates, Cambridge University Press, Cambridge, 2017, https://doi.org/10.1017/9781139016476.
[5] T. Peng, C. Sun, S. Feng, Y. Zhang, F. Fan, Temporal and spatial variation of anthropogenic heat in the central urban area: a case study of Guangzhou, China, ISPRS Int. J. Geo-Inf. 10 (2021), https://doi.org/10.3390/ijgi10030160.
[6] Y. Zhou, Q. Weng, K.R. Gurney, Y. Shuai, X. Hu, Estimation of the relationship between remotely sensed anthropogenic heat discharge and building energy use, ISPRS J. Photogrammetry Remote Sens. 67 (2012) 65–72, https://doi.org/10.1016/j.isprsjprs.2011.10.007.
[7] S. Chapman, J.E.M. Watson, A. Salazar, M. Thatcher, C.A. McAlpine, The impact of urbanization and climate change on urban temperatures: a systematic review, Landsc. Ecol. 32 (2017) 1921–1935, https://doi.org/10.1007/S10980-017-0561-4.
[8] D.J. Sailor, A review of methods for estimating anthropogenic heat and moisture emissions in the urban environment, Int. J. Climatol. 31 (2011) 189–199, https://doi.org/10.1002/joc.2106.

[9] D. Hu, L. Yang, J. Zhou, L. Deng, Estimation of urban energy heat flux and anthropogenic heat discharge using aster image and meteorological data: case study in Beijing metropolitan area, J. Appl. Remote Sens. 6 (2012), 063559, https://doi.org/10.1117/1.jrs.6.063559. –1.

[10] W. Xu, M.J. Wooster, C.S.B. Grimmond, Modelling of urban sensible heat flux at multiple spatial scales: a demonstration using airborne hyperspectral imagery of Shanghai and a temperature-emissivity separation approach, Remote Sens. Environ. 112 (2008) 3493–3510, https://doi.org/10.1016/j.rse.2008.04.009.

[11] Y. Zhang, H. Balzter, X. Wu, Spatial-temporal patterns of urban anthropogenic heat discharge in Fuzhou, China, observed from sensible heat flux using Landsat TM/ETM+ data, Int. J. Rem. Sens. 34 (2013) 1459–1477, https://doi.org/10.1080/01431161.2012.718465.

[12] W.S. Nie, T. Sun, G.H. Ni, Spatiotemporal characteristics of anthropogenic heat in an urban environment: a case study of Tsinghua Campus, Build. Environ. 82 (2014) 675–686, https://doi.org/10.1016/j.buildenv.2014.10.011.

[13] A. Krpo, F. Salamanca, A. Martilli, A. Clappier, On the impact of anthropogenic heat fluxes on the urban boundary layer: a two-dimensional numerical study, Boundary-Layer Meteorol. 136 (2010) 105–127, https://doi.org/10.1007/s10546-010-9491-2.

[14] Y. Liu, Z. Luo, S. Grimmond, Revising the definition of anthropogenic heat flux from buildings: role of human activities and building storage heat flux, Atmos. Chem. Phys. Discuss. (2021) 1–31, https://doi.org/10.5194/acp-2021-914.

[15] X. Ao, C.S.B. Grimmond, H.C. Ward, A.M. Gabey, J. Tan, X.Q. Yang, D. Liu, X. Zhi, H. Liu, N. Zhang, Evaluation of the surface urban energy and water balance scheme (SUEWS) at a dense urban site in shanghai: sensitivity to anthropogenic heat and irrigation, J. Hydrometeorol. 19 (2018) 1983–2005, https://doi.org/10.1175/JHM-D-18-0057.1.

[16] L. Allen, F. Lindberg, C.S.B. Grimmond, Global to city scale urban anthropogenic heat flux: model and variability, Int. J. Climatol. 31 (2011) 1990, https://doi.org/10.1002/joc.2210. –2005.

[17] J. Wen, J.I. Chen, W. Lin, B. Jiang, S. Xu, J. Lan, Impacts of anthropogenic heat flux and urban land-use change on frontal rainfall near coastal regions: a case study of a rainstorm over the pearl river Delta, South China, J. Appl. Meteorol. Climatol. 59 (2020) 363–379, https://doi.org/10.1175/JAMC-D-18-0296.1.

[18] A. Sharma, H.J.S. Fernando, J. Hellmann, F. Chen, Sensitivity of WRF Model to Urban Parameterizations, with Applications to Chicago Metropolitan Urban Heat Island, 2014. http://rda.ucar.edu/datasets/ds083.2/.

[19] Y. Zhao, L. Zhong, Y. Ma, Y. Fu, M. Chen, W. Ma, C. Zhao, Z. Huang, K. Zhou, WRF/UCM simulations of the impacts of urban expansion and future climate change on atmospheric thermal environment in a Chinese megacity, Clim. Change 169 (2021), https://doi.org/10.1007/s10584-021-03287-7.

[20] S. Kato, Y. Yamaguchi, Analysis of urban heat-island effect using ASTER and ETM+ Data: separation of anthropogenic heat discharge and natural heat radiation from sensible heat flux, Remote Sens. Environ. 99 (2005) 44–54, https://doi.org/10.1016/j.rse.2005.04.026.

[21] S.D. Chakraborty, Y. Kant, D. Mitra, Assessment of land surface temperature and heat fluxes over Delhi using remote sensing data, J. Environ. Manag. 148 (2013) 143–152, https://doi.org/10.1016/j.jenvman.2013.11.034.

[22] N. Chrysoulakis, M. Marconcini, J.-P. Gastellu-Etchegorry, C.S.B. Grimmond, C. Feigenwinter, F. Lindberg, F. Del Frate, J. Klostermann, Z. Mitraka, T. Esch, L. Landier, A. Gabey, E. Parlow, F. Olofson, Anthropogenic heat flux estimation from space: results of the first phase of the URBANFLUXES project, Remote Sens. Technol. Appl. Urban Environ. 10008 (2016) 100080C, https://doi.org/10.1117/12.2239411.

[23] S. Ziaul, S. Pal, Anthropogenic heat flux in English Bazar town and its surroundings in West Bengal, India, Remote Sens. Appl. Soc. Environ. 11 (2018) 151–160, https://doi.org/10.1016/j.rsase.2018.06.003.

[24] M.S. Wong, J. Yang, J. Nichol, Q. Weng, M. Menenti, P.W. Chan, Modeling of anthropogenic heat flux using HJ-1B Chinese small satellite image: a study of heterogeneous urbanized areas in Hong Kong, Geosci. Rem. Sens. Lett. IEEE 12 (2015) 1466–1470, https://doi.org/10.1109/LGRS.2015.2409111.

[25] T. Nitis, G. Tsegas, N. Moussiopoulos, D. Gounaridis, D. Bliziotis, Satellite Data Based Approach for the Estimation of Anthropogenic Heat Flux over Urban Areas, 2017, p. 74, https://doi.org/10.1117/12.2280826.

[26] S. Kato, Y. Yamaguchi, Estimation of storage heat flux in an urban area using ASTER data, Remote Sens. Environ. 110 (2007) 1–17, https://doi.org/10.1016/j.rse.2007.02.011.

[27] K. Gupta, P. Garg, P.K. Gupta, A. Debnath, A. Roy, Y. Shukla, An innovative approach for retrieval of gridded urban canopy parameters using very high resolution optical satellite stereo, Int. J. Rem. Sens. 43 (2022) 4378–4409, https://doi.org/10.1080/01431161.2022.2112108.

[28] Census of India, district census handbook - NCT of Delhi, Delhi. https://censusindia.gov.in/, 2001.

[29] Census of India, district census handbook - NCT of Delhi, Delhi. https://censusindia.gov.in/, 2011.

[30] A.T. Hamid, M. Sharif, M.L. Ahmed, Evaluation of Trends in Meteorological Data of Delhi, 2013, pp. 117–124.

[31] C.S.B. Grimmond, T.R. Oke, Aerodynamic properties of urban areas derived from analysis of surface form, J. Appl. Meteorol. 38 (1999) 1262–1292.

[32] F. Lindberg, C. Grimmond, A. Gabey, B. Huang, C.W. Kent, T. Sun, N.E. Theeuwes, H.C. Ward, I. Capel-Timms, Y. Chang, P. Jonsson, N. Krave, D. Liu, D. Meyer, K.G. Frans Olofson, J. Tan, L. Xue, Z. Zhang, Urban Multi-Scale Environmental Predictor (UMEP): an Integrated Tool for City-Based Climate Services, 2017, https://doi.org/10.1016/j.envsoft.2017.09.020.

[33] A. Jhaldiyal, K. Gupta, P.K. Gupta, P. Thakur, P. Kumar, Urban Morphology Extractor: a spatial tool for characterizing urban morphology, Urban Clim. 24 (2018) 237–246, https://doi.org/10.1016/j.uclim.2018.04.003.

[34] T. Gál, J. Unger, Detection of ventilation paths using high-resolution roughness parameter mapping in a large urban area, Build. Environ. 44 (2009) 198–206, https://doi.org/10.1016/j.buildenv.2008.02.008.

[35] R. Waters, R. Allen, W. Bastiaanssen, R. Waters, R. Trezza, W. Bastiaanssen, Surface Energy Balance Algorithms for Land, 2002.

[36] A.A.F. Beg, A.H. Al-Sulttani, A. Ochtyra, A. Jarocińska, A. Marcinkowska, Estimation of evapotranspiration using SEBAL algorithm and landsat-8 data—a case study: tatra mountains region, J. Geol. Resour. Eng. 4 (2016) 257–270, https://doi.org/10.17265/2328-2193/2016.06.002.

[37] B.R. Nikam, F. Ibragimov, A. Chouksey, V. Garg, S.P. Aggarwal, Retrieval of land surface temperature from Landsat 8 TIRS for the command area of Mula irrigation project, Environ. Earth Sci. 75 (2016) 1–17, https://doi.org/10.1007/s12665-016-5952-3.

[38] X. Yu, X. Guo, Z. Wu, Land surface temperature retrieval from landsat 8 TIRS-comparison between radiative transfer equation-based method, split window algorithm and single channel method, Rem. Sens. 6 (2014) 9829–9852, https://doi.org/10.3390/rs6109829.

[39] M. Montanaro, J. Barsi, A. Lunsford, S. Rohrbach, B. Markham, Performance of the thermal infrared sensor on-board landsat 8 over the first year on-orbit, Earth Obs. Syst. XIX. 9218 (2014), 921817, https://doi.org/10.1117/12.2063457.

[40] R.G. Allen, L.S. Pereira, D. Raes, M. Smith, W. Ab, Guidelines for computing crop water requirements - FAO, Rome, Italy. https://www.fao.org/3/x0490e/x0490e00.htm, 1998.

[41] K. Nishida, R.R. Nemani, S.W. Running, J.M. Glassy, An operational remote sensing algorithm of land surface evaporation, J. Geophys. Res. Atmos. 108 (2003), https://doi.org/10.1029/2002jd002062.

[42] B. Tran, J. Van Der Kwast, S. Seyoum, R. Uijlenhoet, G. Jewitt, Uncertainty assessment of satellite remote sensing-based evapotranspiration estimates : a systematic review of methods and gaps, EGUsphere 2023 (2023) 1–40, https://doi.org/10.5194/egusphere-2023-725.

[43] K. Gupta, P. Garg, A. Roy, Assessment of Spatio-Temporal and Diurnal Urban Heat Island Intensities in Delhi Urban Agglomeration Using a High Resolution Weather Research and Forecasting Model, AGU Fall Meet, 2021, p. 2021.

[44] A. Theethai Jacob, A. Jayakumar, K. Gupta, S. Mohandas, M.A. Hendry, D.K.E. Smith, T. Francis, S. Bhati, A.N. Parde, M. Mohan, A.K. Mitra, P. Kumar Gupta, P. Chauhan, R.K. Jenamani, S. Ghude, Implementation of the urban parameterization scheme in the Delhi model with an improved urban morphology, Q. J. R. Meteorol. Soc. 149 (2023) 40–60, https://doi.org/10.1002/qj.4382.

[45] S. Heiple, D.J. Sailor, Using building energy simulation and geospatial modeling techniques to determine high resolution building sector energy consumption profiles, Energy Build. 40 (2008) 1426–1436, https://doi.org/10.1016/j.enbuild.2008.01.005.